Computational Insights into the Inhibition Mechanism of Xanthine Oxidoreductase by Oxipurinol

Yazdan Maghsoud,[1] Chao Dong,[2] and G. Andrés Cisneros*,[1,3]

[1]*Department of Chemistry and Biochemistry, The University of Texas at Dallas, Richardson, TX 75080, USA*

[2]*Department of Chemistry and Physics, The University of Texas Permian Basin, Odessa, TX 79762, USA*

[3]*Department of Physics, The University of Texas at Dallas, Richardson, TX 75080, USA*

*E-mail: andres@utdallas.edu

ABSTRACT

Xanthine oxidoreductase (XOR) is a molybdopterin-containing enzyme found in many living organisms. Its function is to convert hypoxanthine to xanthine and subsequently to urate, which are the final steps in purine elimination in humans. Elevated uric acid levels in the human body can cause gout and hyperuricemia. Therefore, drug development efforts targeting this enzyme are a primary focus not only to treat these conditions but also for other diseases. Oxipurinol, an analog of xanthine, was the drug that emerged as a "gold standard" inhibitor of XO in the late sixties. Crystallographic studies have shown direct coordination of oxipurinol to the molybdenum cofactor (MoCo). The proposed inhibition mechanism based on available crystal structures posits that the oxipurinol's nitrogen replaces a water-exchangeable OH ligand of the Mo atom. However, the detailed steps involved in the inhibition mechanism remain undefined, which would provide important insights for designing more efficacious drugs with similar inhibition functions. In this study, the inhibition mechanism of XOR by oxipurinol is investigated via molecular dynamics (MD) and quantum mechanics/molecular mechanics (QM/MM) calculations. The structural and dynamical effects of oxipurinol on the pre-catalytic structure of the metabolite-bound system are presented, as well as the modeled reaction mechanism catalyzed by the MoCo center in the active site. The kinetics and thermodynamics of the proposed reaction mechanism as well as the non-covalent interactions with the binding cavity align with experimental findings. Our results also suggest the suitability of the inhibition reaction via another tautomer of oxipurinol other than the experimentally predominant tautomer. This might suggest possible routes for designing new analogs of oxipurinol with a similar coordination mode to the latter tautomer, which could lead to more energetically favorable inhibitors.

KEYWORDS: Xanthine Oxidoreductase, Oxipurinol, Molecular Dynamics, Energy Decomposition Analysis, Quantum Mechanics/Molecular Mechanics, Inhibition Mechanism.

1 INTRODUCTION

Xanthine oxidoreductase (XOR) enzymes accelerate the hydroxylation of various substrates containing different functional groups such as aldehyde, purine, and pyrimidine. XOR proteins have been isolated from many organisms.[1-10] The active form of bovine XOR is a homodimer of molecular mass 290 kDa, where each subunit catalyzes the hydroxylation reaction independently.[11-13] As shown in **Figure 1**, each monomer has two iron-sulfur clusters (Fe_2–S_2 or FES), each bridged to four cysteine residues, one flavin adenine dinucleotide coenzyme (FAD), and one molybdopterin cofactor (MoCo). XOR proteins are highly homologous and consist of approximately 1,330 amino acids. For example, the sequence identity between the bovine milk (1,332 residues) and the human liver enzyme (1,333 residues) is about 90 percent.[14, 15] Proteolysis of mammalian XOR with trypsin and comparative sequence alignment indicated that the enzyme is divided into three fragments. The two FES clusters are located in the N-terminal fragment (20 kDa), the FAD is placed in the intermediate 40-kDa fragment, and the MoCo center is located in the C-terminal fragment with a molecular mass of 85 kDa (see **Figure 1**).[16]

XOR is one of the most studied flavoproteins and the redox reaction catalyzed in the heart of this enzyme is well established.[17-24] Mechanistically, the hydroxylation reaction occurs at the MoCo center of XOR and involves the reduction of Mo(VI) to Mo(IV).[11] After completing the reduction half-reaction at the MoCo, the electrons transfer via the FES clusters to the FAD cofactor to complete the oxidative half-reaction by the physiological electron acceptor, NAD^+ or O_2.[16]

Unlike other lower mammals such as cats and dogs, higher apes and humans lack a functional uricase gene that oxidizes urate into water-soluble allantoin.[25, 26] Thus, uric acid is the final, irreversible product of purine breakdown by human XOR, which is excreted by the kidneys and intestinal tract, although it can be accumulated in certain diseases. [27, 28] Several clinical studies showed that hyperuricemia, the aftermath of elevated levels of uric acid in serum, leads to gout and is associated with other medical conditions such as diabetes, cardiovascular disease, metabolic syndrome, and the formation of kidney stones.[29-37] Thus, uric acid excretion has to be increased, or its production by XOR needs to be reduced to decrease the blood concentration of uric acid, and consequently treat these diseases.[38-41] The latter approach has been used to develop several drugs for this target.[41-47]

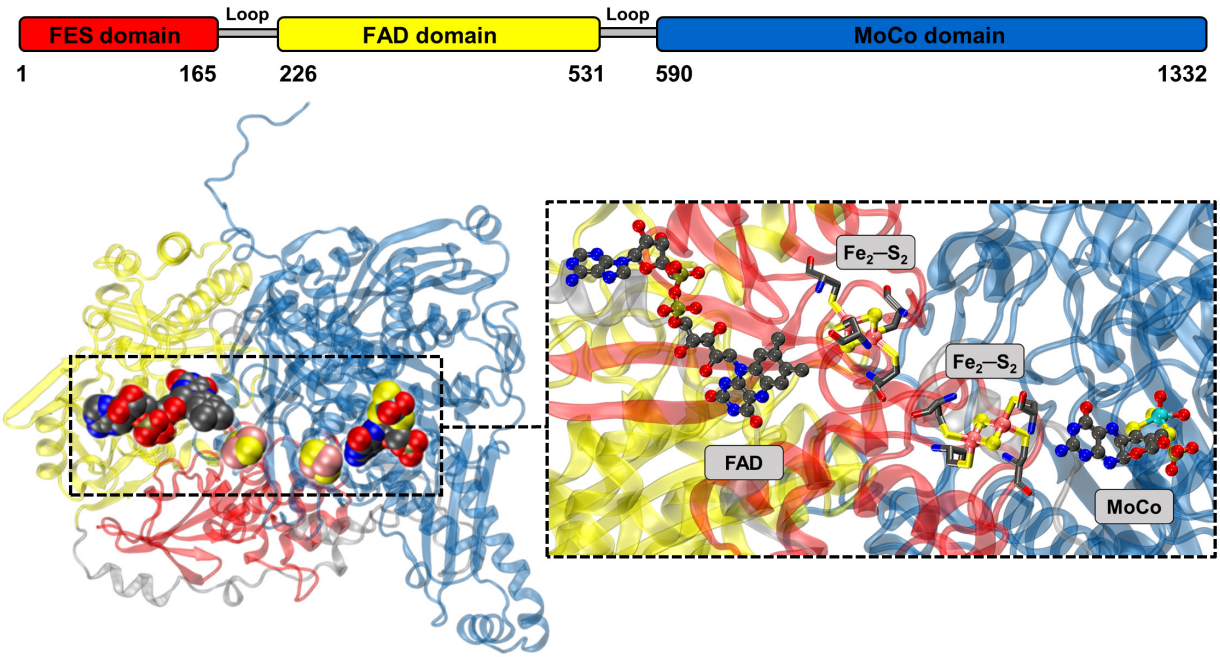

Figure 1. One subunit of the bovine xanthine oxidoreductase homodimer (PDB ID: 1JRO).[48] The magnified close-up represents the XOR's active regions in the redox reaction that are almost linearly positioned in the order of Molybdenum cofactor (MoCo), iron-sulfur clusters (Fe_2–S_2), and the flavin adenine dinucleotide (FAD). Hydrogen atoms are not presented for more clarity, and four cysteine residues bound to the irons of each Fe_2–S_2 cluster are shown in the sticks.

Allopurinol, an analog of hypoxanthine, emerged as an effective inhibitor of xanthine oxidase.[49-51] Later, Massey et al.[52] realized that the active isomer, which effectively inhibits the XOR, is the hydroxylated form of allopurinol, i.e., oxipurinol (see **Scheme 1A**). Oxipurinol has been considered the "gold standard" inhibitor of xanthine and has been widely prescribed ever since due to its excellent pharmacokinetic properties. However, the short dissociation half-life of five hours[52] often leads to a high-dose prescription, causing drastic side effects such as joint pain,[53] severe skin, mucous membrane rash (Steven-Johnson syndrome),[54, 55] acute febrile neutrophilic dermatosis (Sweet's syndrome),[56] toxic epidermal necrolysis,[54, 57] fulminant hepatitis,[58, 59] and even renal failure in rare cases.[60, 61] Due to the drawbacks, researchers worldwide have been designing more effective and longer-lasting inhibitors.[62-75] Among the proposed candidates, BOF-4272,[66, 67, 76] Febuxostat,[69, 77-79] Piraxostat,[71, 80, 81] and Topiroxostat[70, 74, 82-85] have been studied more extensively due to their promising inhibitory effects (see the chemical structures in **Scheme 1A**). Nevertheless, the search for new drugs continues[86-93] due to the increasing number of gout cases worldwide.[94-96]

The mechanism of the catalytic hydroxylation of XO's natural substrates, i.e., xanthine and hypoxanthine, and other purine- or non-purine-based inhibitors, has been extensively investigated by several experimental[97-105] and computational[106-115] studies. This mechanism involves a proton transfer from MoCo to E1261 as shown in **Scheme 1B**. Subsequently, the MoCo's negatively charged oxygen attacks the substrate's carbon adjacent to a N atom, with a transfer of "hydrogen and a negative charge" to the sulfido ligand (=S), and a concomitant reduction of the molybdenum cation from Mo(VI) to Mo(IV).[105, 109,

[110, 116] Subsequently, the enzymatic turnover is fulfilled by an incoming water molecule, leading to $2H^+$ and $2e^-$ release during the oxidation half reaction.[117-119] It has been reported that the "hydrogen and a negative charge" transfer occurs in the form of a hydride ion.[11, 24, 109, 110, 116]

QM/MM studies by Cerqueira and co-workers[112] on the catalytic mechanism of XO with xanthine suggested that a hydrogen atom ($H^{\bullet}$) transfers to the sulfido group, while the second electron is transferred via the oxo-bridge. Hybrid spectroscopic/electronic structure studies by Kirk and co-workers[120, 121] on purine-, non-purine, and aldehyde-based substrates also supported this mechanism. Our previous QM/MM study on the inhibition mechanism of the XO by topiroxostat and its hydroxylated metabolites (drug code: FYX-051) also suggested that the transferred hydrogen to the terminal sulfido at the transition state is nearly neutral and the other electron is transferred via the Mo–O–C bridge.[122]

As mentioned earlier, it had been envisaged that the allopurinol binds to the MoCo center in competition with xanthine. However, it eventually became clear that the inhibition is more complicated and continues in a time-dependent manner, in which the allopurinol acts as a suicide inhibitor to produce oxipurinol.[52, 98] Two crystallographic studies by Truglio et al.[48] and Nishino and co-workers[123] indicated that the reduced bovine milk XOR can be covalently bound to oxipurinol via the N8 atom of the substrate, which is a different coordination mode compared with other previously studied inhibitors (see **Scheme 1C** left). Another study by Nishino and co-workers[124] on the crystal structure of the reduced bovine milk XOR with trihydroxy-FYX-051 (the final hydroxylated metabolite of the topiroxostat family) showed similar coordination, in which the inhibitor is directly coordinated to the molybdenum atom via the nitrogen atom on the cyano group of the inhibitor (see **Scheme 1C** right). Nishino and co-workers concluded that the nitrogen atom of the oxipurinol and the cyano nitrogen of trihydroxy-FYX-051 replace the water-exchangeable hydroxy ligand of the MoCo.

Allopurinol and topiroxostat (FYX-051) are two of the most clinically administered drugs for gout and hyperuricemia. In addition, the last metabolite of each drug forming the Mo–N complex has been identified as the inhibitor form that results in the reduction of uric acid levels in the body. Therefore, to develop more potent and efficient drugs with similar inhibition traits, it is crucial to gain a deeper understanding of the catalytic reaction mechanism involved in the last step of each drug. We extensively investigated the reaction mechanism of topiroxostat in our previous study, including its final metabolite.[122] Herein, we have studied the thermodynamics and kinetics of the inhibition reaction of XO by oxipurinol using classical molecular dynamics and quantum mechanics/molecular mechanics to determine the details of the reaction mechanism for inhibition of XOR by this drug. The remainder of the paper is as follows; in the next section, we describe the approach for the MD and QM/MM simulations, including the structural, dynamical, binding affinity, and energy decomposition analyses, as well as the reaction path optimization and kinetic studies. Subsequently, the results are presented and discussed, followed by concluding remarks.

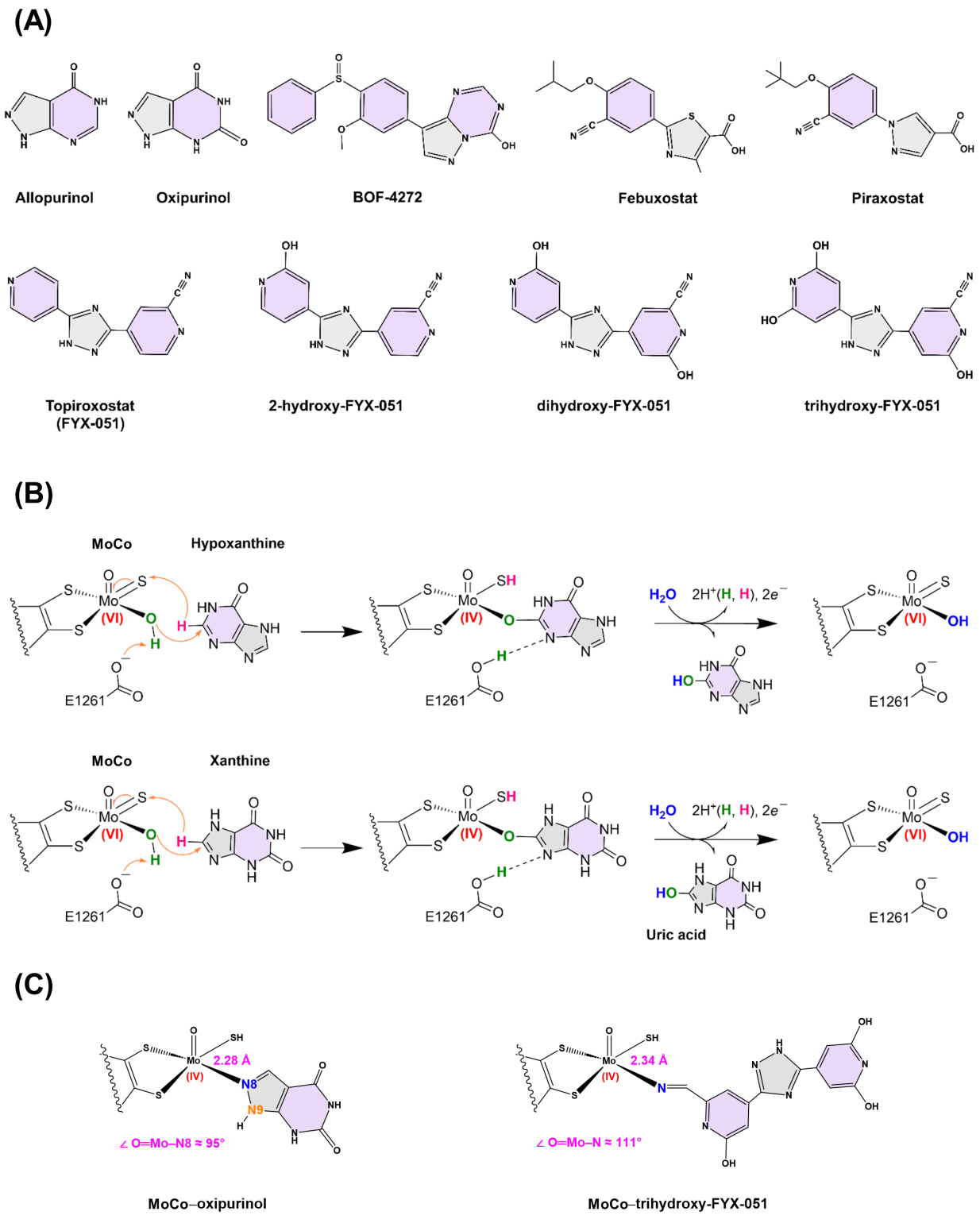

Scheme 1. (A) Some of the known XOR inhibitors: allopurinol and oxipurinol, BOF-4272, febuxostat, piraxostat, and topiroxostat family. **(B)** Proposed reaction mechanisms for the hydroxylation of hypoxanthine and xanthine in the active site of XOR. **(C)** Coordination modes in Left: MoCo–oxipurinol with a direct Mo–N8 bond (PDB IDs: 1JRP & 3BDJ).[48, 123] and Right: MoCo–trihydroxy-FYX-051 with a Mo–N≡C bond (PDB ID: 3AM9).[74]

2 COMPUTATIONAL METHODS

2.1 Molecular Dynamics (MD)

Structural model. The crystal structure of reduced bovine milk xanthine oxidoreductase bound to oxipurinol (PDB ID: 3BDJ)[123] was used for constructing the initial model. The similarity between the human XOR[105, 125] and the bovine isoform is around 90%. The employed PDB had missing fragments, including residues 1, 2, 165–192, 529–536, and 1318–1325, which comprise about 3% of the entire protein. These missing amino acids are located in flexible loops of the XO's surface and far from the active site. Comparative modeling of XO's 3D structure and incorporation of the missing residues was performed using MODELLER 10.1.[126, 127] Further assessments were made by CASP[128] and CAMEO[129] to evaluate the accuracy of the constructed models. Finally, the best-fitted PDB structure was selected for further MD simulations (see **Figure S1**).

MD setup. The parameterization protocol applied for the flavin adenine dinucleotide (FAD) and iron-sulfur cluster (FES) have been described previously.[122] However, the reduced form of molybdenum cofactor and oxipurinol needed to be parameterized (see **Figure S2**). The AMBER force field parameters calculated by Ramos and co-workers[130] were modified by the `MCPB.py` module[131] to obtain the parameters for the reduced MoCo (parameters provided in the SI), in which Mo(VI) is replaced by Mo(IV) and =S ligand is replaced by –SH (termed MoCo in the remainder of the paper). The oxipurinol substrate was parameterized via the R.E.D. server[132-135] and ANTECHAMBER.[136, 137] The protonation of all the amino acid residues was assessed via the PROPKA.[138, 139] Based on the findings by Truglio et al.[48] and Nishino and co-workers,[105, 123, 124] residues E802 and E1261 (key residues in the active site) are both protonated in the reduced XOR.

The LEaP module[140] of AMBER21[141] was used to construct the canonical structures of solvated apo-XO and XO–oxipurinol by adding hydrogen atoms, neutralizing the system with chloride counterions, and solvating the neutralized structure in a cubic box of TIP3P[142] water, extended at least 12 Å from the protein surface. The interactions between the atoms of the system were described with the protein's ff14SB[143] and general GAFF[136] force fields.

The `pmemd.cuda` module[144] of AMBER21 was utilized for conducting MD simulations. To perform minimization, positional restraints with a force constant of 100 kcal mol^{-1} $Å^{-2}$ were applied to all solute molecules. The minimization process consisted of 5000 cycles using steepest descent method, followed by 5000 cycles with conjugate gradient. Subsequently, the system was subjected to MD under constant volume and temperature[145] with all bonds involving hydrogen atoms constrained with SHAKE.[145] The system underwent further minimization in seven steps, each consisting of 5000 MD steps with a time step of 1 fs with 100 kcal mol^{-1} $Å^{-2}$ restraint on the solute's heavy atoms. This process was conducted under constant pressure conditions, using the Berendsen barostat, with the temperature maintained at 10 K.[146] In the next step, each system was heated to 310 K using Langevin dynamics[147-149] with a collision frequency of 2 ps^{-1} followed by 85 ns of NVT equilibration with decreasing restraint (50.0–0.0 kcal mol^{-1} $Å^{-2}$) on the protein's

heavy atoms. Lastly, unrestrained NPT ensemble[147, 149] simulations using a Langevin thermostat and Berendsen barostat[146, 150] were carried out for 500 ns and 1 μs on three replicas, producing a total of 1.5 μs and 3.0 μs of simulation data for the apo-XO and XO–oxipurinol, respectively. Temperature was held constant at 310 K and pressure at 1.0 bar with a 2 fs time step. Long-range Coulomb interactions were approximated using the smooth particle mesh Ewald method[144, 151] and the Van der Waals long-range interactions were approximated with the default isotropic correction implemented in AMBER, using a 10 Å cutoff for non-bonded interactions. All bonds containing hydrogen atoms were treated with SHAKE.

Structural analysis. The CPPTRAJ[152] module of AMBER21 was utilized for analyzing the production dynamics. Normal mode analysis was performed using the ProDy code.[153] Python libraries, namely NumPy, Matplotlib, Pandas, and statsmodels module, along with the Gnuplot program were used for further data processing and two-dimensional plot graphing. MD simulations of replicates for each system were stable without significant fluctuations (see **Figures S3**–**S11**). The generated ensembles were used for clustering analysis. For the clustering analysis, 300,000 frames of the last 400 ns of all three replicates were subjected to multi-dimensional analysis via the *k*-means algorithm[154] implemented in CPPTRAJ. The clustering dimensions corresponded to essential distances and angles between MoCo, oxipurinol, E802, and E1261. Initially, 30 representatives in ten clusters were obtained to identify the frames closest to each cluster's centroid. Later, eight representatives from the four clusters with the highest population abundance and the best orientations of the mentioned residues were selected for QM/MM optimizations (see **Figures S12** and **S13** and **Table S1**).

MM/GBSA analysis. Relative binding energies between oxipurinol and XO for two different tautomers were estimated using the molecular mechanics/Generalized Born surface area (MM/GBSA) approach.[155-157] Calculations were carried out on the last 100,000 frames of each of the three replicates. A comprehensive explanation of the procedure utilized to compute the binding enthalpies had been previously provided.[122] The entropic contributions were not included in the calculations due to convergence issues; however, it has been shown that comparing the relative binding affinities of similar ligands via the MM/GB(PB)SA techniques can achieve satisfactory accuracy, even if the conformational entropy is neglected.[158-166]

2.2 Quantum Mechanics/Molecular Mechanics (QM/MM)

QM/MM setup. QM/MM calculations were performed using LICHEM,[167, 168] to interface Gaussian16[169] (for the QM region) and TINKER[170] (for the MM environment). The QM region was modeled using the ωB97X-D/def2-SVP[171, 172] level of theory, while the MM environment was described using the AMBER ff14SB force field. The QM subsystem consisted of 145 atoms, including the MoCo, oxipurinol, Q767, E802, R880, F914, F1009, E1261, and water molecules within 3 Å of the substrate (see **Figure S14**). The ff14SB potential was employed to describe the remaining residues and solvent molecules. The reduced MoCo was

tested for various multiplicities. Our calculations indicate that the most stable state corresponds to a singlet multiplicity, in agreement with Cerqueira and co-workers[112] and our previous study,[122].

After optimizing the chosen representatives, the reactant with the lowest QM/MM optimization energy was deemed the most stable, and the product was designed based on that structure. The resulting product structure was then subjected to QM/MM calculations using the same level of theory. The potential energy surface of the reaction path between the optimized reactant and product was obtained using the quadratic string method (QSM) combined with the restrained-MM optimization approach implemented in LICHEM.[168] Detailed explanations of the QM/MM calculation protocols can be found in our previous study.[122]

The reactants with the lowest QM/MM optimization energies were employed to calculate QM/MM interaction energies ($IE_{QM/MM}$) between the oxipurinol and XO via the following approach:[173]

$$IE_{QM/MM} = [QM^{active\ site+OXI} - (QM^{active\ site} + QM^{OXI})] + [MM^{XO-OXI} - MM^{apoXO}] \quad \textbf{Eq. 1}$$

The terms $QM^{active\ site+OXI}$, $QM^{active\ site}$, and QM^{OXI} correspond to the single point energies of the QM subsystem, the active site only (MoCo, Q767, E802, R880, F914, F1009, E1261, and $3H_2O$), and the tautomer of interest, respectively. The terms MM^{XO-OXI} and MM^{apoXO} correspond to the MM energies of the XO–OXI and apo-XO, respectively. The basis set superposition error (BSSE) correction is included in the $IE_{QM/MM}$ calculations using the counterpoise approach.[174, 175]

Kinetic parameters based on the calculated critical structures were obtained using Eyringpy.[176] The critical points were approximated by using the QM/MM-optimized structures and obtaining the frequencies and thermochemistry using only the electrostatically-embedded system. These structures were then used for vibrational analysis at the same levels of theory to investigate the kinetics of the reaction via the Eyringpy code.[177] One negative imaginary frequency was seen for the approximate TS corresponding to the motion along the reaction coordinate (see animations in the SI). The rate constants (k_{cat}) and the activation Gibbs free energies ($\Delta G^{\ddagger}$) of the approximate TS in solvent were computed at 310 K and pH 7.0 based on the transition state theory (TST) corrected by the Collins–Kimball theory[178] as implemented in Eyringpy.

NCI and ELF analyses. Non-covalent interactions (NCI) between oxipurinol and the binding pocket residues were analyzed using the pro-molecular density method,[179] as implemented in the Multiwfn V. 3.8 program.[180] 5000 random snapshots from the last 100 ns of MD for the first replicate of each tautomer was used to analyze the electron density and its gradient norm during the dynamics, which allowed for the study of the averaged non-covalent interaction (aNCI) regions. In addition, the QM/MM-optimized structures of the reactant, product, and the approximate TS, were used to generate wavefunctions and calculating grid data of the reduced density gradient (RDG), which allowed for the study the non-covalent interactions (NCI) during the catalytic reaction. NCI surfaces were generated using the RGB color code to illustrate the strength of the interactions. Green and blue surfaces represented strong and weak interactions, such as hydrogen bonds and van der Waals (vdW) forces, while any repulsive interactions were depicted in red.

The NCI surfaces were visualized with an isovalue of 0.4 a.u and a color scale of –0.05 a.u < sign(λ_2)ρ < 0.05 a.u. The QM/MM-optimized coordinates of the critical structures were also used to obtain all the wave functions for the electron localization function (ELF) analysis.[181] The basin analysis[182, 183] feature of Multiwfn V. 3.8[180] was employed to carry out the ELF calculations. The basin illustration was performed using a cubic grid of 200 a.u. with an isovalue of 0.8 a.u. and medium quality grid with a spacing of 0.10 Bohr. The images were rendered using Visual molecular dynamics (VMD).[184]

2.3 Energy Decomposition Analysis (EDA)

EDA calculates the averaged energies of the non-bonded intermolecular interactions as a function of a reference residue(s). The nature of the intermolecular interactions between the protein and any fragment(s) of interest can be studied by this technique, which can be used to qualitatively asses the catalytic roles of individual amino acid residues.[122, 166, 185] Herein, an in-house Fortan90-based EDA code[186-188] was employed on the MD to study the intermolecular effects of the XO on the dynamics and kinetics of the inhibition by oxipurinol. To study the oxipurinol-bound pre-catalytic structure, EDA was run on 25,000 randomly selected snapshots of the 3 μs of the MD simulations from all three replicates. The total difference in the non-bonded intermolecular interaction energy between the MoCo and the protein environment during the MD simulation, ΔE_{NB}, can be calculated as:

$$\Delta E_{NB} = \langle E_{NB} \rangle_{XO-OXI} - \langle E_{NB} \rangle_{apo-XO} \qquad \textbf{Eq. 2}$$

where $\langle E_{NB} \rangle_{XO-OXI}$ and $\langle E_{NB} \rangle_{apo-XO}$ represent the average of non-bonded intermolecular interactions between the MoCo and each residues of the MM environment for the XO–oxipurinol and the apo-XO, respectively.

3 RESULTS AND DISCUSSION

3.1 Dynamics of the Pre-catalytic Inhibition

Xanthine and oxipurinol (also known as alloxanthine) are structurally related purine analogs that differ in the nature of their five-membered heterocyclic rings. Xanthine contains an imidazole ring, while oxipurinol features a pyrazole ring (see **scheme 1**). Like xanthine, oxipurinol can exist as a mixture of tautomers (see **Figure S15**). Several reports on the chemical synthesis of oxipurinol have demonstrated that tautomer-1 represents the predominant tautomeric form of this compound.[49, 189-194] *In vitro* and *in vivo* studies have also suggested that tautomer-1 is the functional derivative of oxipurinol with biological activity.[195-200] Moreover, Truglio et al.[48] suggested that the N9 nitrogen of oxipurinol (see **Scheme 1C** left) in their XDH–oxipurinol inhibited crystal structure from *Rhodobacter capsulatus* (PDB ID: 1JRP) is presumably as NH and forms a hydrogen bond to E730 (identical to E1261 in bovine XO). Hernández et al.[201] computationally showed that among the probable tautomers of oxipurinol, di-keto tautomers (tautomers 1 and 2) are favorable in the gas

phase and aqueous solution. In contrast, the keto–enol (tautomers 3–6) and di-enol (tautomers 7 and 8) forms are very unstable and largely disfavored. However, their results suggest that tautomer-1 is less favorable than tautomer-2 by ~ 3 kcal mol^{-1}.

It should be noted that experimental studies on allopurinol also show that the N9-protonated tautomer is the predominant form of neutral allopurinol.[202-204] In addition, another computational study by Hernández et al.[194] on allopurinol showed that the N9-protonated tautomer of this inhibitor is the predominant form in both the gas phase and aqueous solution with the population of 99% and 88%, respectively. Given the collective findings, it is more likely that tautomer-1 in **Figure S15** is the principal inhibitor of xanthine oxidoreductase.

In our previous study on FYX-051 metabolites, we noticed that the incoming inhibitor exerts proximal and distal impacts on the movements of the enzyme.[122] It is observed in both the previous and the current study that the movements of the FES and FAD domains are non-correlated in the apo-XO (results are obtained from two different crystal structures), while the MoCo domain's movements are anti-correlated (see **Figure 2A**). Moreover, in our previous study, the inhibited enzyme's movements underwent significant changes following the binding of the inhibitor. Specifically, the MoCo domain displayed mostly correlated motions, whereas the other two domains exhibited varying movements in response to each metabolite. Herein, we aimed to investigate whether oxipurinol exhibits comparable effects on the enzyme movements and if there are any similarities between this inhibitor and trihydroxy-FYX-051, which has a similar mode of complexation to XO (see **Scheme 1C**). Interestingly, similar to trihydroxy-FYX-051, the binding of oxipurinol results in a mostly non-correlated FES domain and completely anti-correlated FAD. Moreover residues of the MoCo domain remain correlated with the molybdenum cofactor, except for the areas adjacent to the FAD domain, which become non-correlated (**Figure 2B**). Taken together, our results indicate that ligand binding considerably affects the dynamics of the MoCo domain.

Root-mean-squared deviations and atomic fluctuations for all the systems depicted in **Figures S3**–**S8** show that significant movements primarily occur in the flexible loops of the protein's surface or on the modeled missing residues. The modeled residues were excluded from the principal component analysis (PCA); however, it is still evident that the largest PCA fluctuations are mainly centered around the removed residues and the flexible loops. The PCA results in **Figures S3**–**S8** also indicate that the first two normal modes account for over 90% of the systems' movement modes in all structures. As the first normal mode makes up more than 75% of the movement modes for all structures, it was utilized to interpret the systems (refer to the animations in the SI). **Figure 2A**&**B** and the NMA animations in the SI also reveal that the directionality of the first normal mode's movements in the FES and FAD domains of apo-XO and XO–OXI are similar. Interestingly, the movements of the FES and FAD domains are smaller in magnitude for XO–OXI compared with apo-XO (see animations in the SI). The motion of the MoCo domain are similar between apo-XO and XO–OXI in some regions. Similar to the other two domains, the MoCo domain of apo-XO has larger movements than the inhibited-XO. Combining our observations with those of our previous

investigation,[122] we suggest that oxipurinol, similar to trihydroxy-FYX-051, significantly enhances the stability of the MoCo domain.

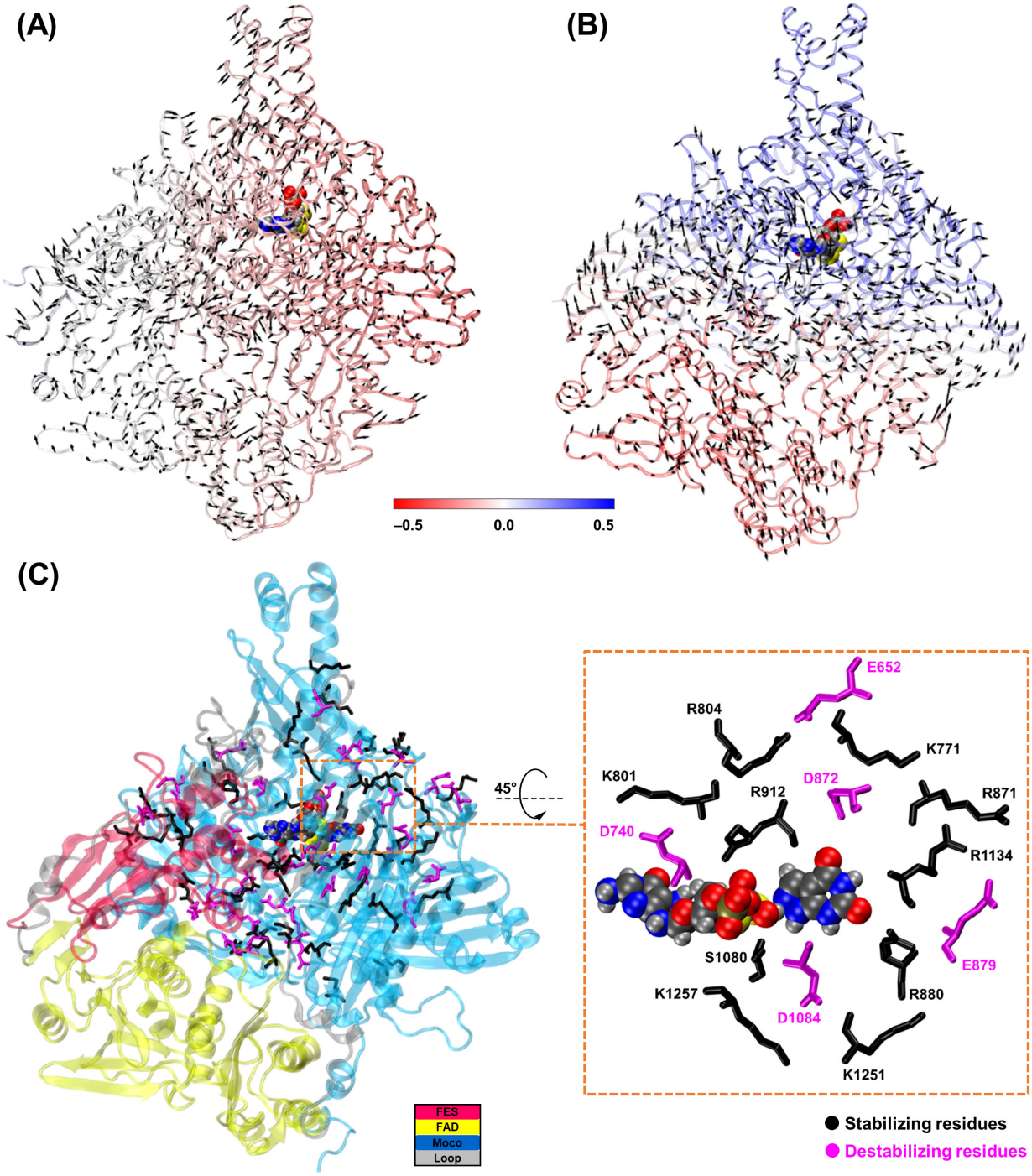

Figure 2. Plot of the principal component analysis on the root-mean-square fluctuations (first mode) along with the residue-wise correlation with respect to molybdenum cofactor as a heatmap projected on the protein for the **(A)** apo-XO and **(B)** XO–OXI. The black arrows show the fluctuations greater than 1.0 Å and point toward the direction of the highest ranked eigenvector and their amplitude is directly proportional to the length of the arrow. Areas with correlated movements in the heatmap are colored blue (0.5), non-correlated areas are white (0.0), and areas with anti-correlated movements are red (–0.5). The first replicate of each MD simulation was used for both analysis. **(C)** Representation of

the residues with considerable non-bonded intermolecular interactions ($|\boldsymbol{\Delta E_{NB}}|$ ≥ 12.0 kcal mol^{-1}) with the molybdenum cofactor of XO–OXI compared to the apo-XO as the reference.

Another helpful method for assessing the role of the enzyme's residues in the MoCo active site is to examine inter-molecular interactions via an energy decomposition analysis (EDA). Here, we focused on a comparative investigation of the impact on the MoCo between the apo and inhibited structure to see whether oxipurinol stabilizes the MoCo domain. The difference of the non-bonded intermolecular interactions (ΔE_{NB}) between the protein and the MoCo was calculated with respect to the apo-XO as the reference to study the intermolecular effects of oxipurinol (see **Table S2)**. In addition, **Figure 2C** provides a three-dimensional illustration of the residues that exhibit significant non-bonded interactions with the MoCo.

The calculated value of the sum of the individual calculated non-bonded interactions, $\sum \Delta E_{NB} \sim$ –174 kcal mol^{-1} suggests a strong attractive interaction between the protein and oxipurinol. Moreover, **Figure 2C** shows that in addition to the MoCo domain's residues, several residues in the FES domain show significant stabilizing/destabilizing contributions to ΔE_{NB}. On the other hand, the FAD domain residues do not appear to have any substantial intermolecular interaction changes (**Table S2**).

We were also interested to see which residues around the active site considerably contribute to the reaction center of the oxipurinol-bound system consisting of MoCo, oxipurinol, and E1261—which are directly involved in the inhibition reaction. Calculated values of E_{NB} in **Table S3** reveals several positively and negatively charged residues with $|E_{NB}|$ ≥ 30 kcal mol^{-1}, which respectively stabilize or destabilize the active site during the MD simulation. **Figure 3A** illustrates residues with significant intermolecular interactions that are located in the active site's first and second coordination shells. As can be seen, several residues such as R829, R839, R871, R880, R899, K902, R912, K1045, K1052, S1080, R1134, K1250, and K1251 display significant stabilizing interactions with the active site, while negatively charged residues, D740, D745, D872, E879, E1037, D1084, E1092, E1196, E1209, and E1210 contribute to destabilization. Oxipurinol is predominantly surrounded by stabilizing contributors, among which R839 and R880 show substantial stabilizing effects ($E_{NB} \sim$ –61 and –80 kcal mol^{-1}, respectively). In contrast, MoCo is mostly surrounded by destabilizing residues with only two residues, R912 and K1045, providing significantly large stabilizing interactions ($E_{NB} \sim$ –143 and –105 kcal mol^{-1}, respectively).

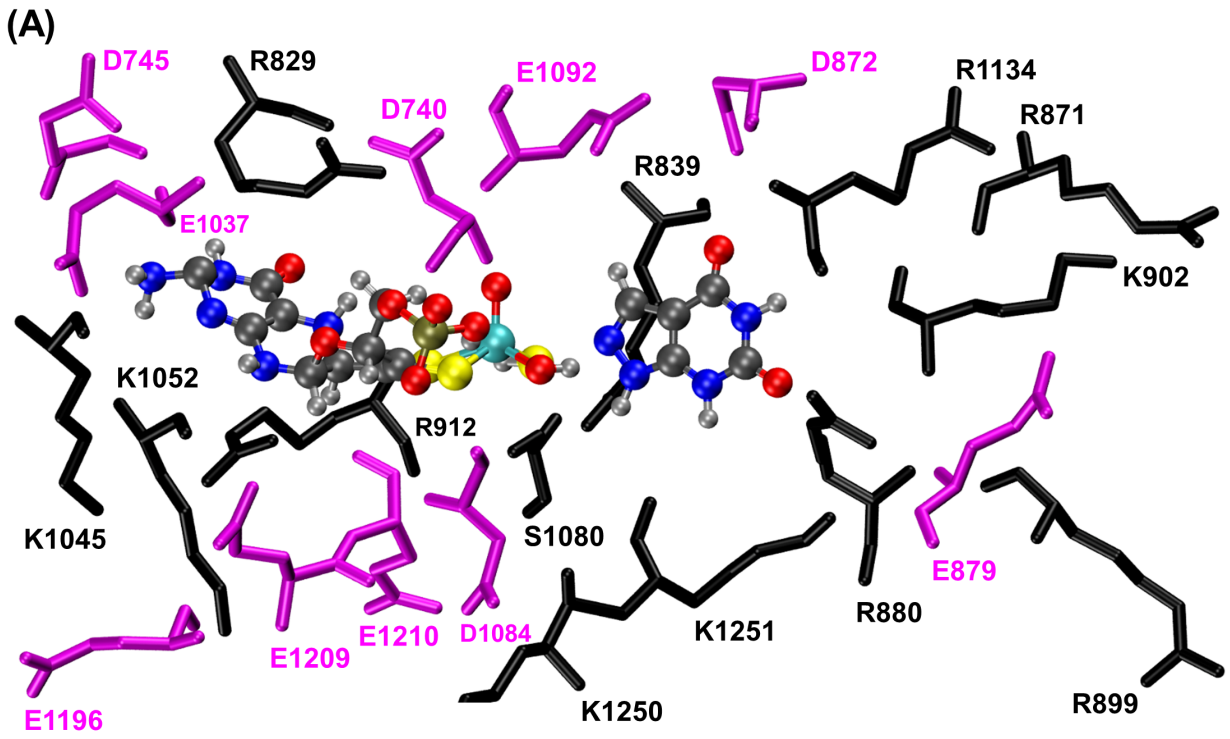

Approximate Region	Stabilizing		Destabilizing	
	Residue	E_{NB}	Residue	E_{NB}
Surrounding Oxipurinol	R839	–61	D872	52
	R871	–50	E879	50
	R880	–80		
	R899	–31		
	K902	–32		
	R1134	–44		
	K1251	–47		
Surrounding MoCo	R829	–57	D740	62
	R912	–143	D745	73
	K1045	–105	E1037	84
	K1052	–42	D1084	73
			E1196	59
			E1209	61
			E1210	40
Interface	S1080	–38	E1092	86
	K1250	–59		

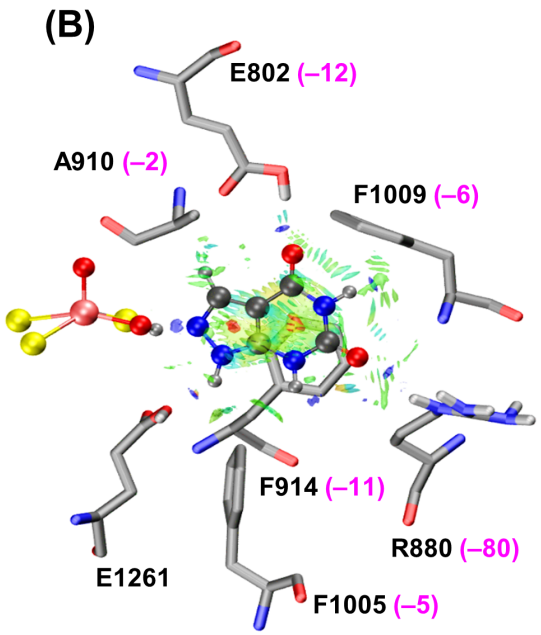

Figure 3. (A) Residues of the first and the second coordination shell of the XO–OXI active site with considerable non-bonded intermolecular interactions ($|E_{NB}| \geq 30$ kcal mol^{-1}). Residues in the sticks have stabilizing (black) and destabilizing (purple) interactions with the active site, given in the ball-and-sticks. E1261 of the active site is not shown for enhanced clarity. **(B)** Plot of the aNCI between the inhibitor and the surrounding residues of the active site. Values in parenthesis correspond to E_{NB} (kcal mol^{-1}) of each residue.

A plot of the average non-covalent interactions (aNCI) along the dynamics simulation is shown in **Figure 3B**, illustrating the residues of the binding pocket having interacting surfaces with oxipurinol. Several

residues including E802, R880, A910, F914, F1005, F1009, and E1261 have attraction interactions (in the NCI scale) with the inhibitor in the binding pocket. Interestingly, in addition to R880 that exhibited a substantial stabilizing effect in our EDA analysis, all the other residues seen in the aNCI also have stabilizing contribution to the active site, especially E802 and F914 ($E_{NB} \sim$ –12 and –11 kcal mol^{-1}, respectively). Taken together with the EDA, these results are consistent with an overall stabilizing environment of the protein in the binding pocket, promoting the binding of XO–OXI. Moreover, as shown in **Figure 3A** and **Table S3**, unprotonated aspartate and glutamate residues have destabilizing contributions to the MoCo active site. The stabilizing effect of the protonated E802 and its non-covalent interaction with the inhibitor, which were also observed in our previous study on topiroxostat,[122] agrees with the experimental results assuming the priority of protonated E802 over the negatively charged glutamate.[48, 105, 123, 124]

As discussed in the beginning of this section, the di-keto isomer of oxipurinol is more stable than the other forms. Many studies have also supported that tautomer-1 (see **Figure S15**) is the primary product of synthesis and, thus, the active form of oxipurinol in inhibiting XOR. However, a computational study by Hernández et al.[201] has suggested tautomer-2 as a possible alternative. Therefore, this tautomeric form has also been studied here as a theoretically probable inhibitor, termed OXI$^{T\text{-}2}$, for the rest of the paper.

The binding affinities (ΔH_{bind}) between the inhibitor and the enzyme during the dynamics of the pre-catalytic reaction were calculated via the MM/GBSA approach (see **Table S4**). Calculated ΔH_{bind} values for the major (OXI) and the theoretical tautomer (OXI$^{T\text{-}2}$) are –24.5 and –25.8 kcal mol^{-1}, respectively, showing a slightly greater binding affinity for the later one. The QM/MM interaction energies ($IE_{QM/MM}$) between the inhibitor and the XO were also studied, which are –120.0 and –124.2 kcal mol^{-1}, respectively, showing a similar trend as the binding affinities. Components of the QM/MM interaction energies (E_{QM} and E_{MM} of **Eq. 1**) in **Table S5**, suggest that despite the slight difference between $IE_{QM/MM}$ values, the differences between E_{QM} and E_{MM} for the tautomers are significant. The values of E_{QM} and E_{MM} for the major tautomer are similar (–58.9 and –61.1 kcal mol^{-1}, respectively), implying its interaction with the enzyme is moderately stabilized by the active site (E_{QM}) and the solvated enzyme (E_{MM}). On the other hand, the E_{QM} value is more than twice that of E_{MM} for XO and the theoretical tautomer (–84.2 and –40.0 kcal mol^{-1}, respectively), suggesting its interaction is mainly stabilized by the MoCo active site.

Taken together, the results of the binding affinities and interaction energies of these two forms propose the probability of a higher propensity of the theoretical tautomer to interact with the enzyme if presented in the active site.

3.2 Catalytic Inhibition Reaction

Several studies have concluded that oxipurinol coordinates to the reduced MoCo during the enzymatic turnover.[52, 124, 205] However, extensive investigations by Spector and co-workers on both bovine and human

xanthine oxidase provided particularly strong evidence that the reduced enzyme is susceptible to the inhibition by oxipurinol.[101, 199, 206, 207] They realized that the enzyme undergoes inactivation when electron donors like xanthine and allopurinol substrates or the chemical reductant dithionite are present. In contrast, there is no inactivation in the absence of electron donors or when an artificial electron acceptor capable of directly re-oxidizing the MoCo is present. Moreover, Nishino and co-workers proposed that the XO–OXI complexation occurs in the presence of a proton.[124] Given that the XO–OXI complexation takes place during enzymatic turnover and a proton is required at the reaction center, which can be provided by E1261, a possible mechanism associated with this process, as depicted in **Scheme 2**, was investigated.

The proposed mechanism for oxipurinol is similar to the suggested mechanism for trihydroxy-FYX-051,[122] in which the water-exchangeable hydroxyl ligand is replaced by the nitrogen atom to form a stable complex. However, the pathway for the MoCo–OXI complexation involves the protonation of hydroxide ion (OH^-) by E1261, followed by the release of a water molecule (see animation in the SI). The resulting complex dissociates by a replacement of oxipurinol by an incoming water molecule, resulting in the re-oxidation of the molybdenum to its original oxidation state, fulfilling the enzymatic turnover.

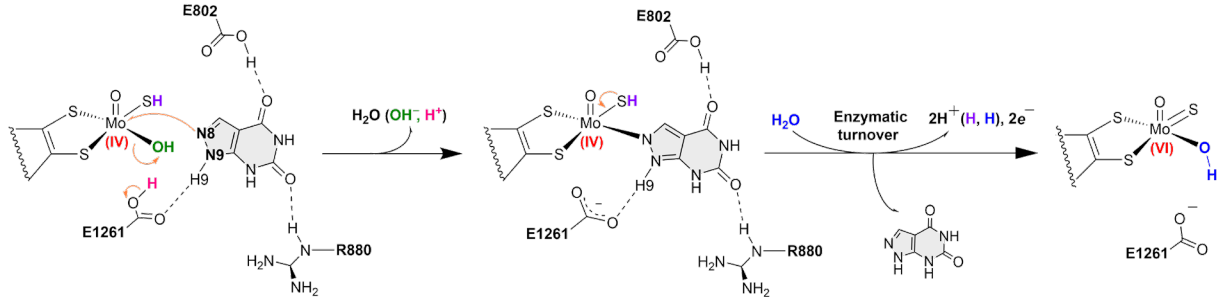

Scheme 2. Studied mechanism for the catalytic inhibition of XO by oxipurinol.

The results in **Figure 5A** suggest that the reaction is slightly endergonic (ΔE_{react} = 1.0 kcal mol^{-1} and ΔG_{react}= 1.6 kcal mol^{-1}). As shown in **Figure 5C**, the creation of V(Mo,N8) and V(O,Hε) ELF disynaptic basins in the product (bead 15) with electron populations of 3.1 e^- and 1.8 e^-, respectively, imply the formation of the MoCo–oxipurinol complex and a water molecule at this point (refer to **Table S6** for the detailed values). The calculated energy barrier associated with the approximate TS (corresponding to bead 9) is 27.6(29.8) kcal mol^{-1}. At this point of the reaction mechanism, the Mo–OH bond cleaves while the proton transfers from E1261 to the cleaving hydroxyl (Mo…OH…H…Glu), and the Mo…N8 bond forms between the MoCo and oxipurinol. The creation of ELF trisynaptic basins V(Mo,N8,C), V(Mo,O,H), and V(O,Hε,Oε1) with electron populations of 2.7 e^-, 3.1 e^-, and 1.7 e^- at bead 9 also suggest the formation of the approximate TS at this point.

The QM/MM-optimized geometries of the key structures involved in the complexation reaction shown in **Figure 5B** provide calculated values for the O–Mo–N angle and Mo–N distance in the product, which are 96° and 2.32 Å, respectively. These values are consistent with the experimental data from the referenced crystal structure with the reported values of 94.97° and 2.28 Å. Moreover, the RMSD of the active site's

atoms and the RMSD of the protein's backbone atoms with respect to the crystal structure are 1.3 Å and 3.1 Å, respectively. These distances, coupled with the blue surfaces of the NCIs in **Figure 5A**, suggest that oxipurinol maintains hydrogen bonds with N768, R880, E1261, and two water molecules throughout the catalytic reaction pathway. In addition, the blue NCI surfaces between the N8 nitrogen of oxipurinol and the hydrogen of MoCo's hydroxyl ligand in shows a hydrogen bond between them. The presence of a hydrogen bond, combined with the cleavage of the hydroxyl ligand from the MoCo, may account for the relatively high barrier energy observed in both experiments and our calculations.

A larger view of the NCIs in **Figure 5A** is provided in **Figure S16** showing the non-covalent interactions between the binding pocket residues with the reactant and product. This figure highlights the important role of some residues such as E802, L873, R880, A910, F914, F1009, A1078, A1079, and E1261. In conjunction with the previous results of aNCI and EDA, R839, K902, F1005, S1080, and K1251 also play essential roles in the pre-catalytic and catalytic inhibition of XO by oxipurinol.

Considering the effects of the mentioned non-bonded contributions to the MoCo's active site (both EDA and NCI) and comparing these results to the experimental mutagenesis studies showing the impacts of each mutation on XO function, we can obtain further insights into the residues with significant effects on the XO inhibition. As listed in **Table S7**, several studies have demonstrated that mutagenesis of E802,[105, 208, 209] R880,[105, 210-213] and E1261[105, 211] showing substantial non-bonded interactions in our analyses leads to complete loss of XO function. Our EDA and NCI results also show proximal stabilizing effects by residues such as G799,[212] R912,[214] and A1079,[212] whose mutagenesis leads to partial or total loss of XO function. Similar experimental effects were seen upon mutating R149,[215] H884,[212] and N887[212] with distal stabilizing effects in our EDA. Moreover, several clinical trials on human cases showed the substantial impact of residues R228,[216] R606,[217] K721,[218] R824,[213] and R1282[219] on lowering the XO activity (hypouricemia). Our EDA results show significant stabilizing effects of these residues on the active site. EDA results also suggest the destabilizing effects of residues I702, H1220, and T909 on the active site, suggesting their mutation might promote the function of XO. Interestingly, clinical studies demonstrate the increasing activity of XO upon the mutation of these residues.[215, 217] Overall, our results are consistent with experimental mutagenesis studies, and the predicted effects of residues within the binding pocket could be considered for developing analogs of oxipurinol with improved inhibitory effects.

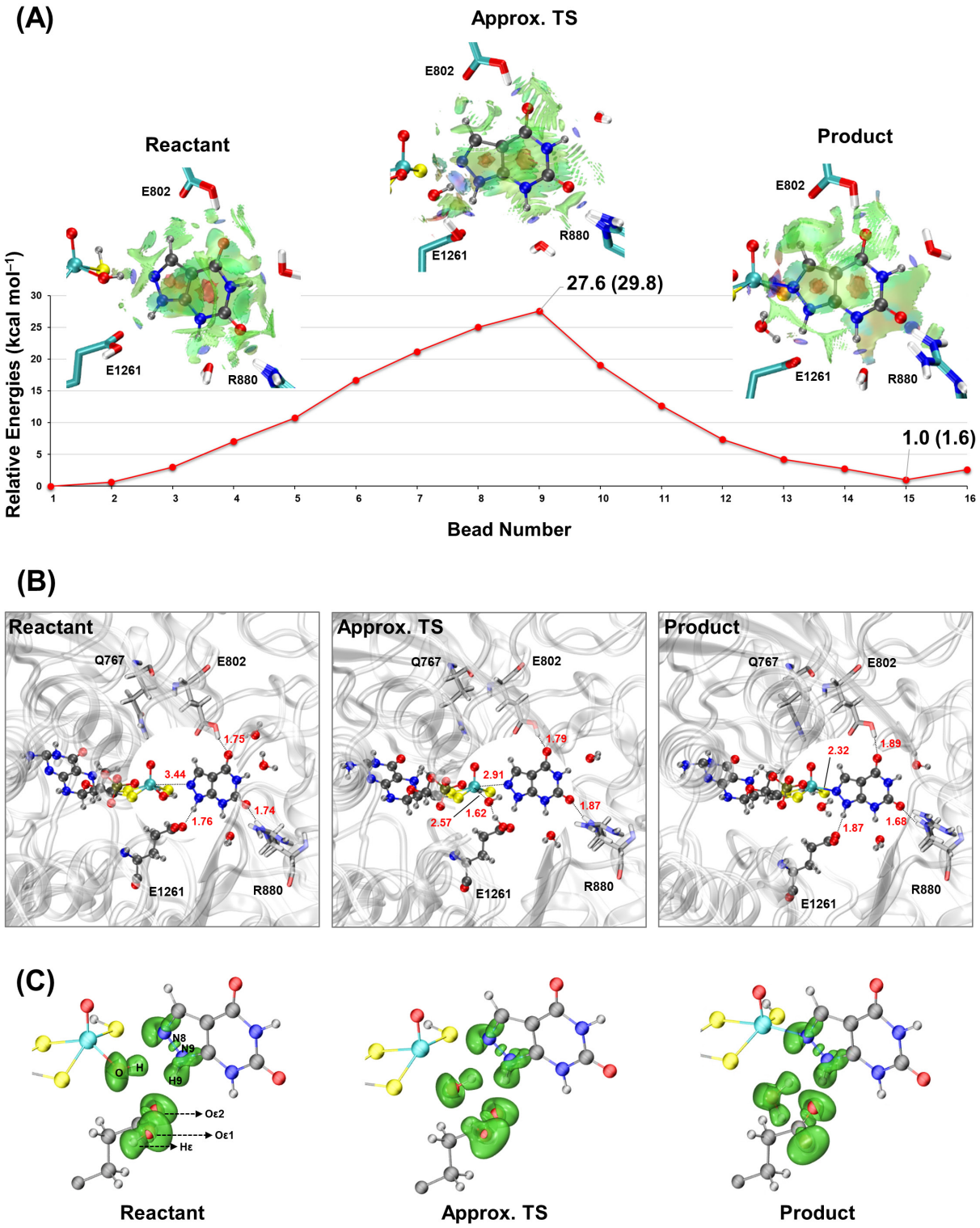

Figure 4. (A) The minimum energy path for the catalytic inhibition of XO by oxipurinol modeled via the QSM together with the NCI plots of the critical structures. The QM/MM optimization energies (kcal mol^{-1}) are calculated at the ωB97X-D/def2-SVP level of theory with AMBER ff14SB force field. The values in parenthesis correspond to the Gibbs free energies obtained from the vibrational analysis using Eyringpy. **(B)** The optimized geometries of the critical structures with the values of selected distances (Å). **(C)** The ELF basins among the MoCo, oxipurinol, and E1261 for the critical structures along the reaction pathway.

The experimental activation energy values for the XO inactivation ($\Delta G^{\ddagger}_{inact}$) by oxipurinol are 31 kcal mol^{-1} and 28 kcal mol^{-1} for human and bovine xanthine oxidase, respectively,[101] which are in good agreement with our calculated barrier free energy using Eyring TST in **Figure 5A** ($\Delta G^{\ddagger}$ = 29.8 kcal mol^{-1}). Moreover, the rate constant (k_{cat}) value calculated via the vibrational analysis is 0.039 s^{-1} for OXI$^{T\text{-}1}$, which also correlates well with the experimental values of 0.03 s^{-1} and 0.02 s^{-1} for the human and bovine xanthine oxidase, respectively.[101]

Several studies have indicated that oxipurinol-inactivated XO can be reactivated at varying rates. The slowest reactivation rate is through spontaneous means.[51, 52] Cycling of the enzyme in the presence of xanthine substrate leads to an intermediate reactivation rate.[206] Finally, the reduced MoCo can be directly reoxidized through artificial electron acceptors, resulting in a quick release of oxipurinol.[52, 220, 221] The experimental activation energy values for the spontaneous reactivation process ($\Delta G^{\ddagger}_{react}$) are 25 kcal mol^{-1} and 27 kcal mol^{-1} for human and bovine XO, respectively.[101] These values are in good agreement with our calculated backward barrier corresponding to 26.6(28.2) kcal mol^{-1}.

It is worth mentioning that our calculated backward barrier ($\Delta E^{\ddagger}_{backward}$) for trihydroxy-FYX-051 in our previous study was 32.6 kcal mol^{-1}, which is ~ 6–7 kcal mol^{-1} larger than oxipurinol. This difference in backward barriers, which reflects the spontaneous reactivation rate of the reduced XO, might be comparable with the observed differences in dissociation half-lives ($t_{1/2}$) between oxipurinol (~ 5 hours)[52] and trihydroxy-FYX-051 (~ 20.4 to 72 hours).[74]

As mentioned before, OXI$^{T\text{-}2}$ was also considered a possible theoretical alternative for the biologically active tautomer. The proposed mechanism for this form, as well as the corresponding reaction path study are provided in Section 13 of the SI (**Figures S17**–**S20**). Interestingly, the inhibition reaction by this form, which involves a spontaneous proton transfer from the tautomer to the hydroxyl ligand of MoCo, is –10.7 kcal mol^{-1} and the energy barrier is 14.8 kcal mol^{-1}. These results suggest that the catalytic inhibition might be more favorable for this tautomer if this molecule (or a similar analog) could be synthesized. This might suggest possible routes for designing new analogs of oxipurinol with a similar coordination mode to this tautomeric form.

4 CONCLUSION

Oxipurinol, the active metabolite of allopurinol, is widely used to treat gout and hyperuricemia as an effective xanthine oxidase inhibitor. However, its inhibition mechanism has not been studied at the atomic level. The MD results show proximal stabilizing effects of the incoming inhibitors on the active site's environment and distal influences on the MoCo, FES, and FAD domains. EDA results suggests several residues located in the first and second coordination shells of the active site with substantial stabilizing effects such as E802, R880, R912, F914, S1080, and K1045. In addition, oxipurinol forms non-covalent interactions with E802, L873, R880, A910, F914, F1005, F1009, A1078, A1079, and E1261 during the pre-

catalytic and catalytic stages of the inhibition. A probable inhibition mechanism was investigated based on the insights provided by previous experimental studies, which turned out to be thermodynamically feasible compared to the experimental observations. The product state for XO–OXI is endergonic with a calculated reaction energy of 1.0 kcal mol^{-1}. The proximity between the experimental activation energy and the rate constant for the enzyme inactivation by oxipurinol ($\Delta G^{\ddagger}_{inact}$= 28 kcal mol^{-1} and k_{cat} = 0.02 s^{-1} for bovine XO) with the calculated energy barrier and the rate constant ($\Delta G^{\ddagger}$ ~ 29.8 kcal mol^{-1} and k_{cat} = 0.039 s^{-1}) suggest that our proposed mechanism may be kinetically feasible. Moreover, our calculated backward barrier is 26.6 kcal mol^{-1}, consistent with the experimental activation energy values for the spontaneous reactivation process ($\Delta G^{\ddagger}_{react}$ = 27 kcal mol^{-1} for bovine XO). Calculated intermolecular interaction results underscore the important role of several residues during the enzyme inhibition process, including E802, L873, R880, A910, F914, F1005, F1009, A1078, A1079, S1080 and E1261, which could be considered as significantly interacting residues that may be exploited for the future development of more potent oxipurinol analogs.

ASSOCIATED CONTENT

Data and Software Availability

All simulations and analyses employed via third-party software are described and referenced in the Computational Methods section. The EDA and LICHEM software programs are available at the Cisneros Research Group GitHub: https://github.com/CisnerosResearch/AMBER-EDA and https://github.com/CisnerosResearch/LICHEM.

Supporting Information

Additional details of MD, EDA, NCI, and QM/MM (PDF)

Additional ESI for the initial coordinates and parameters for all the studied systems (ESI-1.zip)

Videos animating the first principal modes and the reaction paths for each tautomer (ESI-2.ZIP)

CONFLICTS OF INTEREST

The authors declare no conflict of interest.

ACKNOWLEDGMENTS

This study is funded by the NIH Grant No. R01GM108583. Molecular dynamics simulations for this project were performed on the Ganymede2 and Titan HPC clusters at the University of Texas at Dallas' Cyberinfrastructure and Research Services. The QM/MM calculations were implemented on the CASCaM CRUNTCh3 and CRUNTCh4 HPC clusters at the University of North Texas' Chemistry Department, partially

funded by the NSF Grant Nos. CHE1531468 and OAC-2117247. The authors thank Professor Filippo Romiti for insightful discussions.

REFERENCES

1. Pritsos, C. A., Cellular distribution, metabolism and regulation of the xanthine oxidoreductase enzyme system. *Chem. Biol. Interact.* **2000**, 129, 195-208.

2. Garattini, E.; Mendel, R.; Romão, M. J.; Wright, R.; Terao, M., Mammalian molybdo-flavoenzymes, an expanding family of proteins: structure, genetics, regulation, function and pathophysiology. *Biochem. J.* **2003**, 372, 15-32.

3. Hesberg, C.; Hänsch, R.; Mendel, R. R.; Bittner, F., Tandem orientation of duplicated xanthine dehydrogenase genes from Arabidopsis thaliana: differential gene expression and enzyme activities. *J. Biol. Chem.* **2004**, 279, 13547-13554.

4. Yasuhara, A.; Akiba-Goto, M.; Aisaka, K., Cloning and sequencing of the aldehyde oxidase gene from Methylobacillus sp. KY4400. *Biosci. Biotechnol. Biochem.* **2005**, 69, 2435-2438.

5. Mendel, R. R., Biology of the molybdenum cofactor. *J. Exp. Bot.* **2007**, 58, 2289-2296.

6. Zhang, Y.; Gladyshev, V. N., Molybdoproteomes and evolution of molybdenum utilization. *J. Mol. Biol.* **2008**, 379, 881-899.

7. Kurosaki, M.; Bolis, M.; Fratelli, M.; Barzago, M. M.; Pattini, L.; Perretta, G.; Terao, M.; Garattini, E., Structure and evolution of vertebrate aldehyde oxidases: from gene duplication to gene suppression. *Cell. Mol. Life Sci.* **2013**, 70, 1807-1830.

8. Garattini, E.; Terao, M., Aldehyde oxidase and its importance in novel drug discovery: present and future challenges. *Expert Opin. Drug Discovery* **2013**, 8, 641-654.

9. Marelja, Z.; Dambowsky, M.; Bolis, M.; Georgiou, M. L.; Garattini, E.; Missirlis, F.; Leimkühler, S., The four aldehyde oxidases of Drosophila melanogaster have different gene expression patterns and enzyme substrate specificities. *J. Exp. Biol.* **2014**, 217, 2201-2211.

10. Garattini, E.; Terao, M., Xanthine Oxidoreductase and Aldehyde Oxidases. **2018**.

11. Rajagopalan, K.; Johnson, J. L., The pterin molybdenum cofactors. *J. Biol. Chem.* **1992**, 267, 10199-10202.

12. Romão, M. J.; Archer, M.; Moura, I.; Moura, J. J.; LeGall, J.; Engh, R.; Schneider, M.; Hof, P.; Huber, R., Crystal structure of the xanthine oxidase-related aldehyde oxido-reductase from D. gigas. *Science* **1995**, 270, 1170-1176.

13. Xia, M.; Dempski, R.; Hille, R., The reductive half-reaction of xanthine oxidase: reaction with aldehyde substrates and identification of the catalytically labile oxygen. *J. Biol. Chem.* **1999**, 274, 3323-3330.

14. Kimiyoshi, I.; Yoshihiro, A.; Kumi, N.; Shinsei, M.; Tatsuo, H.; Osamu, S.; Nobuyoshi, S.; Takeshi, N., Cloning of the cDNA encoding human xanthine dehydrogenase (oxidase): structural analysis of the protein and chromosomal location of the gene. *Gene* **1993**, 133, 279-284.

15. Berglund, L.; Rasmussen, J.; Andersen, M.; Rasmussen, M.; Petersen, T., Purification of the bovine xanthine oxidoreductase from milk fat globule membranes and cloning of complementary deoxyribonucleic acid. *J. Dairy Sci.* **1996**, 79, 198-204.

16. Hille, R.; Nishino, T., Xanthine oxidase and xanthine dehydrogenase. *FASEB J.* **1995**, 9, 995-1003.

17. Harrison, R., Structure and function of xanthine oxidoreductase: where are we now? *Free Radic. Biol. Med.* **2002**, 33, 774-797.

18. Berry, C. E.; Hare, J. M., Xanthine oxidoreductase and cardiovascular disease: molecular mechanisms and pathophysiological implications. *J. Physiol.* **2004**, 555, 589-606.

19. Alderman, M.; Aiyer, K. J., Uric acid: role in cardiovascular disease and effects of losartan. *Curr. Med. Res. Opin.* **2004**, 20, 369-379.

20. Hille, R., Molybdenum-containing hydroxylases. *Arch. Biochem. Biophys.* **2005**, 433, 107-116.

21. Nishino, T.; Okamoto, K.; Eger, B. T.; Pai, E. F.; Nishino, T., Mammalian xanthine oxidoreductase–mechanism of transition from xanthine dehydrogenase to xanthine oxidase. *FEBS J.* **2008**, 275, 3278-3289.

22. Nossaman, V. E.; Nossaman, B. D.; Kadowitz, P. J., Nitrates and nitrites in the treatment of ischemic cardiac disease. *Cardiol. Rev.* **2010**, 18, 190.

23. Agarwal, A.; Banerjee, A.; Banerjee, U., Xanthine oxidoreductase: a journey from purine metabolism to cardiovascular excitation-contraction coupling. *Crit. Rev. Biotechnol.* **2011**, 31, 264-280.

24. Hille, R.; Nishino, T.; Bittner, F., Molybdenum enzymes in higher organisms. *Coord. Chem. Rev.* **2011**, 255, 1179-1205.

25. Folin, O., THE URIC ACID PROBLEM. AN EXPERIMENTAL STUDY ON ANIMALS AND MAN, INCLUDING GOUTY SUBJECTS.* BY OTTO FOLIN, HILDING BERGLUND, AND CLIFFORD DERICK. *J. Biol. Chem.* **1924**, 60, 361.

26. Shestopalov, A.; Shkurat, T.; Mikashinovich, Z.; Kryzhanovskaya, I.; Bogacheva, M.; Lomteva, S.; Prokof'Ev, V.; Gus'Kov, E., Biological functions of allantoin. *Biology bulletin* **2006**, 33, 437-440.

27. Kelley, E. E.; Khoo, N. K.; Hundley, N. J.; Malik, U. Z.; Freeman, B. A.; Tarpey, M. M., Hydrogen peroxide is the major oxidant product of xanthine oxidase. *Free Radic. Biol. Med.* **2010**, 48, 493-498.

28. Flemmig, J.; Kuchta, K.; Arnhold, J.; Rauwald, H., Olea europaea leaf (Ph. Eur.) extract as well as several of its isolated phenolics inhibit the gout-related enzyme xanthine oxidase. *Phytomedicine* **2011**, 18, 561-566.

29. Obermayr, R. P.; Temml, C.; Gutjahr, G.; Knechtelsdorfer, M.; Oberbauer, R.; Klauser-Braun, R., Elevated uric acid increases the risk for kidney disease. *J. Am. Soc. Nephrol.* **2008**, 19, 2407-2413.

30. Kanbay, M.; Segal, M.; Afsar, B.; Kang, D.-H.; Rodriguez-Iturbe, B.; Johnson, R. J., The role of uric acid in the pathogenesis of human cardiovascular disease. *Heart* **2013**, 99, 759-766.

31. Li, C.; Hsieh, M.-C.; Chang, S.-J., Metabolic syndrome, diabetes, and hyperuricemia. *Curr. Opin. Rheumatol.* **2013**, 25, 210-216.

32. Jalal, D. I., Hyperuricemia, the kidneys, and the spectrum of associated diseases: a narrative review. *Curr. Med. Res. Opin.* **2016**, 32, 1863-1869.

33. El Din, U. A. S.; Salem, M. M.; Abdulazim, D. O., Uric acid in the pathogenesis of metabolic, renal, and cardiovascular diseases: A review. *J. Adv. Res.* **2017**, 8, 537-548.

34. Kuwabara, M.; Niwa, K.; Nishihara, S.; Nishi, Y.; Takahashi, O.; Kario, K.; Yamamoto, K.; Yamashita, T.; Hisatome, I., Hyperuricemia is an independent competing risk factor for atrial fibrillation. *Int. J. Cardiol.* **2017**, 231, 137-142.

35. Johnson, R. J.; Bakris, G. L.; Borghi, C.; Chonchol, M. B.; Feldman, D.; Lanaspa, M. A.; Merriman, T. R.; Moe, O. W.; Mount, D. B.; Lozada, L. G. S., Hyperuricemia, acute and chronic kidney disease, hypertension, and cardiovascular disease: report of a scientific workshop organized by the National Kidney Foundation. *Am. J. Kidney Dis.* **2018**, 71, 851-865.

36. Borghi, C.; Agabiti-Rosei, E.; Johnson, R. J.; Kielstein, J. T.; Lurbe, E.; Mancia, G.; Redon, J.; Stack, A. G.; Tsioufis, K. P., Hyperuricaemia and gout in cardiovascular, metabolic and kidney disease. *Eur. J. Intern. Med.* **2020**, 80, 1-11.

37. Nishikawa, T.; Nagata, N.; Shimakami, T.; Shirakura, T.; Matsui, C.; Ni, Y.; Zhuge, F.; Xu, L.; Chen, G.; Nagashimada, M., Xanthine oxidase inhibition attenuates insulin resistance and diet-induced steatohepatitis in mice. *Sci. Rep.* **2020**, 10, 1-11.

38. Khanna, D.; Fitzgerald, J. D.; Khanna, P. P.; Bae, S.; Singh, M. K.; Neogi, T.; Pillinger, M. H.; Merill, J.; Lee, S.; Prakash, S., 2012 American College of Rheumatology guidelines for management of gout. Part 1: systematic nonpharmacologic and pharmacologic therapeutic approaches to hyperuricemia. *Arthritis Care Res. (Hoboken)* **2012**, 64, 1431-1446.

39. Khanna, D.; Khanna, P. P.; Fitzgerald, J. D.; Singh, M. K.; Bae, S.; Neogi, T.; Pillinger, M. H.; Merill, J.; Lee, S.; Prakash, S., 2012 American College of Rheumatology guidelines for management of gout. Part 2: therapy and antiinflammatory prophylaxis of acute gouty arthritis. *Arthritis Care Res. (Hoboken)* **2012**, 64, 1447-1461.

40. Miner, J. N.; Tan, P. K.; Hyndman, D.; Liu, S.; Iverson, C.; Nanavati, P.; Hagerty, D. T.; Manhard, K.; Shen, Z.; Girardet, J.-L., Lesinurad, a novel, oral compound for gout, acts to decrease serum uric acid through inhibition of urate transporters in the kidney. *Arthritis Res. Ther.* **2016**, 18, 1-10.

41. Tan, P. K.; Liu, S.; Gunic, E.; Miner, J. N., Discovery and characterization of verinurad, a potent and specific inhibitor of URAT1 for the treatment of hyperuricemia and gout. *Sci. Rep.* **2017**, 7, 1-11.

42. Nguyen, M. T. T.; Awale, S.; Tezuka, Y.; Le Tran, Q.; Kadota, S., Xanthine oxidase inhibitors from the heartwood of Vietnamese Caesalpinia sappan. *Chem. Pharm. Bull. (Tokyo)* **2005**, 53, 984-988.

43. Higgins, P.; Ferguson, L. D.; Walters, M. R., Xanthine oxidase inhibition for the treatment of stroke disease: a novel therapeutic approach. *Expert Rev. Cardiovasc. Ther.* **2011**, 9, 399-401.

44. Harrold, L., New developments in gout. *Curr. Opin. Rheumatol.* **2013**, 25, 304-309.

45. Gliozzi, M.; Malara, N.; Muscoli, S.; Mollace, V., The treatment of hyperuricemia. *Int. J. Cardiol.* **2016**, 213, 23-27.

46. Yu, W.; Cheng, J.-D., Uric acid and cardiovascular disease: an update from molecular mechanism to clinical perspective. *Front. Pharmacol.* **2020**, 11, 582680.

47. Yu, Z.; Kan, R.; Wu, S.; Guo, H.; Zhao, W.; Ding, L.; Zheng, F.; Liu, J., Xanthine oxidase inhibitory peptides derived from tuna protein: virtual screening, inhibitory activity, and molecular mechanisms. *J. Sci. Food Agric.* **2021**, 101, 1349-1354.

48. Truglio, J. J.; Theis, K.; Leimkühler, S.; Rappa, R.; Rajagopalan, K.; Kisker, C., Crystal structures of the active and alloxanthine-inhibited forms of xanthine dehydrogenase from Rhodobacter capsulatus. *Structure* **2002**, 10, 115-125.

49. Robins, R. K., Potential purine antagonists. I. Synthesis of some 4, 6-substituted pyrazolo [3, 4-d] pyrimidines1. *J. Am. Chem. Soc.* **1956**, 78, 784-790.

50. Elion, G. B.; Callahan, S.; Nathan, H.; Bieber, S.; Rundles, R. W.; Hitchings, G. H., Potentiation by inhibition of drug degradation: 6-substituted purines and xanthine oxidase. *Biochem. Pharmacol.* **1963**, 12, 85-93.

51. Elion, G. B., Enzymatic and metabolic studies with allopurinol. *Ann. Rheum. Dis.* **1966**, 25, 608.

52. Massey, V.; Komai, H.; Palmer, G.; Elion, G. B., On the mechanism of inactivation of xanthine oxidase by allopurinol and other pyrazolo [3, 4-d] pyrimidines. *J. Biol. Chem.* **1970**, 245, 2837-2844.

53. Hill, E. M.; Sky, K.; Sit, M.; Collamer, A.; Higgs, J., Does starting allopurinol prolong acute treated gout? A randomized clinical trial. *J. Clin. Rheumatol.* **2015**, 21, 120-125.

54. Hasegawa, A.; Abe, R., Recent advances in managing and understanding Stevens-Johnson syndrome and toxic epidermal necrolysis. *F1000Research* **2020**, 9.

55. Halevy, S.; Ghislain, P.-D.; Mockenhaupt, M.; Fagot, J.-P.; Bavinck, J. N. B.; Sidoroff, A.; Naldi, L.; Dunant, A.; Viboud, C.; Roujeau, J.-C., Allopurinol is the most common cause of Stevens-Johnson syndrome and toxic epidermal necrolysis in Europe and Israel. *J. Am. Acad. Dermatol.* **2008**, 58, 25-32.

56. Polimeni, G.; Cardillo, R.; Garaffo, E.; Giardina, C.; Macrì, R.; Sirna, V.; Guarneri, C.; Arcoraci, V., Allopurinol-induced Sweet's syndrome. *Int. J. Immunopathol. Pharmacol.* **2016**, 29, 329-332.

57. Scavone, C.; Di Mauro, C.; Ruggiero, R.; Bernardi, F. F.; Trama, U.; Aiezza, M. L.; Rafaniello, C.; Capuano, A., Severe cutaneous adverse drug reactions associated with allopurinol: an analysis of spontaneous reporting system in Southern Italy. *Drugs-Real World Outcomes* **2020**, 7, 41-51.

58. Singer, J. Z.; Wallace, S. L., The allopurinol hypersensitivity syndrome. Unnecessary morbidity and mortality. *Arthritis Rheum.* **1986**, 29, 82-87.

59. Raper, R.; Ibels, L.; Lauer, C.; Barnes, P.; Lunzer, M., Fulminant hepatic failure due to allopurinol. *Aust. N. Z. J. Med.* **1984**, 14, 63-65.

60. Rødevand, E.; Sletvold, O.; Kvande, K. T., Side effects off allopurinol. *Tidsskr. Nor. Legeforen.* **2004**, 124, 2618-2619.

61. Mackenzie, I. S.; Ford, I.; Nuki, G.; Hallas, J.; Hawkey, C. J.; Webster, J.; Ralston, S. H.; Walters, M.; Robertson, M.; De Caterina, R., Long-term cardiovascular safety of febuxostat compared with allopurinol in patients with gout (FAST): a multicentre, prospective, randomised, open-label, non-inferiority trial. *The Lancet* **2020**, 396, 1745-1757.

62. Hille, R.; Massey, V., Tight binding inhibitors of xanthine oxidase. *Pharmacol. Ther.* **1981**, 14, 249-263.

63. Hawkes, T. R.; George, G. N.; Bray, R., The structure of the inhibitory complex of alloxanthine (1 H-pyrazolo [3, 4-d] pyrimidine-4, 6-diol) with the molybdenum centre of xanthine oxidase from electron-paramagnetic-resonance spectroscopy. *Biochem. J.* **1984**, 218, 961-968.

64. Wortmann, R.; Ridolfo, A.; Lightfoot Jr, R.; Fox, I., Antihyperuricemic properties of amflutizole in gout. *J. Rheumatol.* **1985**, 12, 540-543.

65. Skibo, E. B., Noncompetitive and irreversible inhibition of xanthine oxidase by benzimidazole analogs acting at the functional flavin adenine dinucleotide cofactor. *Biochemistry* **1986**, 25, 4189-4194.

66. Sato, S.; Tatsumi, K.; Nishino, T. A novel xanthine dehydrogenase inhibitor (BOF-4272). In *Purine and pyrimidine metabolism in man VII*; Springer: 1991, pp 135-138.

67. Okamoto, K.; Nishino, T., Mechanism of Inhibition of Xanthine Oxidase with a New Tight Binding Inhibitor (∗). *J. Biol. Chem.* **1995**, 270, 7816-7821.

68. Nagamatsu, T.; Yamasaki, H.; Fujita, T.; Endo, K.; Machida, H., Novel xanthine oxidase inhibitor studies. Part 2. Synthesis and xanthine oxidase inhibitory activities of 2-substituted 6-alkylidenehydrazino- or 6-arylmethylidenehydrazino-7H-purines and 3-and/or 5-substituted 9H-1, 2, 4-triazolo [3, 4-i] purines. *J. Chem. Soc., Perkin Trans. 1* **1999**, 3117-3125.

69. Okamoto, K.; Eger, B. T.; Nishino, T.; Kondo, S.; Pai, E. F.; Nishino, T., An extremely potent inhibitor of xanthine oxidoreductase: crystal structure of the enzyme-inhibitor complex and mechanism of inhibition. *J. Biol. Chem.* **2003**, 278, 1848-1855.

70. Okamoto, K.; Matsumoto, K.; Hille, R.; Eger, B. T.; Pai, E. F.; Nishino, T., The crystal structure of xanthine oxidoreductase during catalysis: implications for reaction mechanism and enzyme inhibition. *Proc. Natl. Acad. Sci. U. S. A.* **2004**, 101, 7931-7936.

71. Fukunari, A.; Okamoto, K.; Nishino, T.; Eger, B. T.; Pai, E. F.; Kamezawa, M.; Yamada, I.; Kato, N., Y-700 [1-[3-Cyano-4-(2, 2-dimethylpropoxy) phenyl]-1H-pyrazole-4-carboxylic acid]: a potent xanthine oxidoreductase inhibitor with hepatic excretion. *J. Pharmacol. Exp. Ther.* **2004**, 311, 519-528.

72. Tamta, H.; Thilagavathi, R.; Chakraborti, A. K.; Mukhopadhyay, A. K., 6-(N-benzoylamino) purine as a novel and potent inhibitor of xanthine oxidase: inhibition mechanism and molecular modeling studies. *J. Enzyme Inhib. Med. Chem.* **2005**, 20, 317-324.

73. Pacher, P.; Nivorozhkin, A.; Szabó, C., Therapeutic effects of xanthine oxidase inhibitors: renaissance half a century after the discovery of allopurinol. *Pharmacol. Rev.* **2006**, 58, 87-114.

74. Matsumoto, K.; Okamoto, K.; Ashizawa, N.; Nishino, T., FYX-051: a novel and potent hybrid-type inhibitor of xanthine oxidoreductase. *J. Pharmacol. Exp. Ther.* **2011**, 336, 95-103.

75. Kumar, R.; Darpan; Sharma, S.; Singh, R., Xanthine oxidase inhibitors: a patent survey. *Expert Opin. Ther. Pat.* **2011**, 21, 1071-1108.

76. Uematsu, T.; Nakashima, M., Pharmacokinetic and pharmacodynamic properties of a novel xanthine oxidase inhibitor, BOF-4272, in healthy volunteers. *J. Pharmacol. Exp. Ther.* **1994**, 270, 453-459.

77. Komoriya, K.; Osada, Y.; Hasegawa, M.; Horiuchi, H.; Kondo, S.; Couch, R. C.; Griffin, T. B., Hypouricemic effect of allopurinol and the novel xanthine oxidase inhibitor TEI-6720 in chimpanzees. *Eur. J. Pharmacol.* **1993**, 250, 455-460.

78. Osada, Y.; Tsuchimoto, M.; Fukushima, H.; Takahashi, K.; Kondo, S.; Hasegawa, M.; Komoriya, K., Hypouricemic effect of the novel xanthine oxidase inhibitor, TEI-6720, in rodents. *Eur. J. Pharmacol.* **1993**, 241, 183-188.

79. Becker, M. A.; Schumacher Jr, H. R.; Wortmann, R. L.; MacDonald, P. A.; Eustace, D.; Palo, W. A.; Streit, J.; Joseph-Ridge, N., Febuxostat compared with allopurinol in patients with hyperuricemia and gout. *N. Engl. J. Med.* **2005**, 353, 2450-2461.

80. Yamada, I.; Fukunari, A.; Osajima, T.; Kamezawa, M.; Mori, H.; Iwane, J., Pharmacokinetics/pharmacodynamics of Y-700, a novel xanthine oxidase inhibitor, in rats and man. *Nucleosides Nucleotides Nucleic Acids* **2004**, 23, 1123-1125.

81. Hashimoto, T.; Fukunari, A.; Yamada, I.; Yanaka, N.; Chen, D.; Kato, N., Y-700, a novel inhibitor of xanthine oxidase, suppresses the development of colon aberrant crypt foci and cell proliferation in 1, 2-dimethylhydrazine-treated mice. *Biosci. Biotechnol. Biochem.* **2005**, 69, 209-211.

82. Shimo, T.; Ashizawa, N.; Moto, M.; Matsumoto, K.; Iwanaga, T.; Nagata, O., FYX-051, a xanthine oxidoreductase inhibitor, induces nephropathy in rats, but not in monkeys. *Toxicol. Pathol.* **2009**, 37, 438-445.

83. Hosoya, T.; Ishikawa, T.; Ogawa, Y.; Sakamoto, R.; Ohashi, T., Multicenter, open-label study of long-term topiroxostat (FYX-051) administration in Japanese hyperuricemic patients with or without gout. *Clin. Drug Investig.* **2018**, 38, 1135-1143.

84. Sato, T.; Ashizawa, N.; Matsumoto, K.; Iwanaga, T.; Nakamura, H.; Inoue, T.; Nagata, O., Discovery of 3-(3-cyano-4-pyridyl)-5-(4-pyridyl)-1, 2, 4-triazole, FYX-051-a xanthine oxidoreductase inhibitor for the treatment of hyperuricemia. *Bioorg. Med. Chem. Lett.* **2009**, 19, 6225-6229.

85. Chen, C.; Lü, J.-M.; Yao, Q., Hyperuricemia-related diseases and xanthine oxidoreductase (XOR) inhibitors: an overview. *Med. Sci. Monit.* **2016**, 22, 2501.

86. Ojha, R.; Singh, J.; Ojha, A.; Singh, H.; Sharma, S.; Nepali, K., An updated patent review: xanthine oxidase inhibitors for the treatment of hyperuricemia and gout (2011-2015). *Expert Opin. Ther. Pat.* **2017**, 27, 311-345.

87. Huneycutt, E.; Board, C.; Clements, J. N., Lesinurad, a selective URAT-1 inhibitor with a novel mechanism in combination with a xanthine oxidase inhibitor, for hyperuricemia associated with gout. *J. Pharm. Pract.* **2018**, 31, 670-677.

88. Masuoka, N.; Kubo, I., Characterization of the xanthine oxidase inhibitory activity of alk (en) yl phenols and related compounds. *Phytochemistry* **2018**, 155, 100-106.

89. Kumar, R.; Joshi, G.; Kler, H.; Kalra, S.; Kaur, M.; Arya, R., Toward an understanding of structural insights of xanthine and aldehyde oxidases: an overview of their inhibitors and role in various diseases. *Med. Res. Rev.* **2018**, 38, 1073-1125.

90. Mehmood, A.; Ishaq, M.; Zhao, L.; Safdar, B.; Rehman, A. u.; Munir, M.; Raza, A.; Nadeem, M.; Iqbal, W.; Wang, C., Natural compounds with xanthine oxidase inhibitory activity: A review. *Chem. Biol. Drug Des.* **2019**, 93, 387-418.

91. Malik, N.; Dhiman, P.; Khatkar, A., In silico and 3D QSAR studies of natural based derivatives as xanthine oxidase inhibitors. *Curr. Top. Med. Chem.* **2019**, 19, 123-138.

92. Luna, G.; Dolzhenko, A. V.; Mancera, R. L., Inhibitors of Xanthine Oxidase: Scaffold Diversity and Structure-Based Drug Design. *ChemMedChem* **2019**, 14, 714-743.

93. Gunduğdu, Ö.; Noma, S. A. A.; Taskin-Tok, T.; Ateş, B.; Kishali, N., Evaluation of xanthine oxidase inhibitor properties on isoindoline-1, 3-dion derivatives and calculation of interaction mechanism. *J. Mol. Struct.* **2020**, 1204, 127523.

94. Chen, L. X.; Schumacher, H. R., Gout: an evidence-based review. *J. Clin. Rheumatol.* **2008**, 14, S55-S62.

95. Richette, P.; Bardin, T., Gout. *The Lancet* **2010**, 375, 318-328.

96. Vos, T.; Barber, R. M.; Bell, B.; Bertozzi-Villa, A.; Biryukov, S.; Bolliger, I.; Charlson, F.; Davis, A.; Degenhardt, L.; Dicker, D., Global, regional, and national incidence, prevalence, and years lived with disability for 301 acute and chronic diseases and injuries in 188 countries, 1990–2013: a systematic analysis for the Global Burden of Disease Study 2013. *The lancet* **2015**, 386, 743-800.

97. Elion, G. B.; Kovensky, A.; Hitchings, G. H.; Metz, E.; Rundles, R. W., Metabolic studies of allopurinol, an inhibitor of xanthine oxidase. *Biochem. Pharmacol.* **1966**, 15, 863-880.

98. Spector, T.; Johns, D., 4-Hydroxypyrazolo (3, 4-d) pyrimidine as a substrate for xanthine oxidase: loss of conventional substrate activity with catalytic cycling of the enzyme. *Biochem. Biophys. Res. Commun.* **1970**, 38, 583-589.

99. Edmondson, D.; Ballou, D.; Van Heuvelen, A.; Palmer, G.; Massey, V., Kinetic studies on the substrate reduction of xanthine oxidase. *J. Biol. Chem.* **1973**, 248, 6135-6144.

100. Olson, J. S.; Ballou, D. P.; Palmer, G.; Massey, V., The mechanism of action of xanthine oxidase. *J. Biol. Chem.* **1974**, 249, 4363-4382.

101. Spector, T.; Hall, W. W.; Krenitsky, T. A., Human and bovine xanthine oxidases: inhibition studies with oxipurinol. *Biochem. Pharmacol.* **1986**, 35, 3109-3114.

102. Mondal, M. S.; Mitra, S., Kinetics and thermodynamics of the molecular mechanism of the reductive half-reaction of xanthine oxidase. *Biochemistry* **1994**, 33, 10305-10312.

103. Stockert, A. L.; Shinde, S. S.; Anderson, R. F.; Hille, R., The reaction mechanism of xanthine oxidase: evidence for two-electron chemistry rather than sequential one-electron steps. *J. Am. Chem. Soc.* **2002**, 124, 14554-14555.

104. Choi, E.-Y.; Stockert, A. L.; Leimkühler, S.; Hille, R., Studies on the mechanism of action of xanthine oxidase. *J. Inorg. Biochem.* **2004**, 98, 841-848.

105. Yamaguchi, Y.; Matsumura, T.; Ichida, K.; Okamoto, K.; Nishino, T., Human xanthine oxidase changes its substrate specificity to aldehyde oxidase type upon mutation of amino acid residues in the active site: roles of active site residues in binding and activation of purine substrate. *Journal of Biochemistry* **2007**, 141, 513-524.

106. Amano, T.; Ochi, N.; Sato, H.; Sakaki, S., Oxidation reaction by Xanthine oxidase. Theoretical study of reaction mechanism. *J. Am. Chem. Soc.* **2007**, 129, 8131-8138.

107. Alfaro, J. F.; Jones, J. P., Studies on the mechanism of aldehyde oxidase and xanthine oxidase. *J. Org. Chem.* **2008**, 73, 9469-9472.

108. Bayse, C. A., Density-functional theory models of xanthine oxidoreductase activity: comparison of substrate tautomerization and protonation. *Dalton Trans.* **2009**, 2306-2314.

109. Metz, S.; Thiel, W., A combined QM/MM study on the reductive half-reaction of xanthine oxidase: substrate orientation and mechanism. *J. Am. Chem. Soc.* **2009**, 131, 14885-14902.

110. Metz, S.; Thiel, W., QM/MM studies of xanthine oxidase: variations of cofactor, substrate, and active-site Glu802. *J. Phys. Chem. B* **2010**, 114, 1506-1517.

111. Du, Y.; Liu, Z.; Qiao, F.; Wang, S.; Chen, K.; Zhang, X., Computational exploration of reactive fragment for mechanism-based inhibition of xanthine oxidase. *J. Organomet. Chem.* **2018**, 864, 58-67.

112. Ribeiro, P. M.; Fernandes, H. S.; Maia, L. B.; Sousa, S. F.; Moura, J. J.; Cerqueira, N. M., The complete catalytic mechanism of xanthine oxidase: a computational study. *Inorg. Chem. Front.* **2021**, 8, 405-416.

113. Bray, M. R.; Deeth, R. J., The catalytic activity of xanthine oxidase: mechanistic insights throughcomputer modelling. *J. Chem. Soc., Dalton Trans.* **1997**, 1267-1268.

114. Zhang, X.-H.; Wu, Y.-D., A theoretical study on the mechanism of the reductive half-reaction of xanthine oxidase. *Inorg. Chem.* **2005**, 44, 1466-1471.

115. Ilich, P.; Hille, R., Mechanism of Formamide Hydroxylation Catalyzed by a Molybdenum− Dithiolene Complex: A Model for Xanthine Oxidase Reactivity. *J. Phys. Chem. B* **1999**, 103, 5406-5412.

116. Maiti, N. C.; Tomita, T.; Kitagawa, T.; Okamoto, K.; Nishino, T., Resonance Raman studies on xanthine oxidase: observation of MoVI-ligand vibrations. *JBIC, J. Biol. Inorg. Chem.* **2003**, 8, 327-333.

117. Schopfer, L. M.; Massey, V.; Nishino, T., Rapid reaction studies on the reduction and oxidation of chicken liver xanthine dehydrogenase by the xanthine/urate and NAD/NADH couples. *J. Biol. Chem.* **1988**, 263, 13528-13538.

118. Kobayashi, K.; Miki, M.; Okamoto, K.; Nishino, T., Electron transfer process in milk xanthine dehydrogenase as studied by pulse radiolysis. *J. Biol. Chem.* **1993**, 268, 24642-24646.

119. Anderson, R. F.; Hille, R.; Massey, V., The radical chemistry of milk xanthine oxidase as studied by radiation chemistry techniques. *J. Biol. Chem.* **1986**, 261, 15870-15876.

120. Kirk, M. L.; Berhane, A., Correlating C□ H Bond Cleavage with Molybdenum Reduction in Xanthine Oxidase. *Chem. Biodivers.* **2012**, 9, 1756-1760.

121. Sempombe, J.; Stein, B.; Kirk, M. L., Spectroscopic and Electronic Structure Studies Probing Covalency Contributions to C–H Bond Activation and Transition-State Stabilization in Xanthine Oxidase. *Inorg. Chem.* **2011**, 50, 10919-10928.

122. Maghsoud, Y.; Dong, C.; Cisneros, G. A., Computational Characterization of the Inhibition Mechanism of Xanthine Oxidoreductase by Topiroxostat. *ACS Catal.* **2023**, Accepted.

123. Okamoto, K.; Eger, B. T.; Nishino, T.; Pai, E. F.; Nishino, T., Mechanism of inhibition of xanthine oxidoreductase by allopurinol: crystal structure of reduced bovine milk xanthine oxidoreductase bound with oxipurinol. *Nucleosides Nucleotides Nucleic Acids* **2008**, 27, 888-893.

124. Okamoto, K.; Kusano, T.; Nishino, T., Chemical nature and reaction mechanisms of the molybdenum cofactor of xanthine oxidoreductase. *Curr. Pharm. Des.* **2013**, 19, 2606-2614.

125. Pearson, A.; Godber, B.; Eisenthal, R.; Taylor, G.; Harrison, R., Human milk xanthine dehydrogenase is incompletely converted to the oxidase form in the absence of proteolysis. *A Structural Explanation* **2006**.

126. Eswar, N.; Eramian, D.; Webb, B.; Shen, M.-Y.; Sali, A. Protein structure modeling with MODELLER. In *Structural proteomics*; Springer: 2008, pp 145-159.

127. Eswar, N.; Webb, B.; Marti-Renom, M. A.; Madhusudhan, M.; Eramian, D.; Shen, M. y.; Pieper, U.; Sali, A., Comparative protein structure modeling using Modeller. *Curr. Protoc. Bioinf.* **2006**, 15, 5.6. 1-5.6. 30.

128. Moult, J.; Fidelis, K.; Kryshtafovych, A.; Schwede, T.; Tramontano, A., Critical assessment of methods of protein structure prediction (CASP)—round x. *Proteins: Struct., Funct., Bioinf.* **2014**, 82, 1-6.

129. Haas, J.; Roth, S.; Arnold, K.; Kiefer, F.; Schmidt, T.; Bordoli, L.; Schwede, T., The Protein Model Portal—a comprehensive resource for protein structure and model information. *Database* **2013**, 2013.

130. Ferreira, P.; Cerqueira, N. M.; Brás, N. F.; Fernandes, P. A.; Ramos, M. J., Parametrization of Molybdenum Cofactors for the AMBER Force Field. *J. Chem. Theory Comput.* **2018**, 14, 2538-2548.

131. Li, P.; Merz Jr, K. M., In; ACS Publications: 2016.

132. Bayly, C. I.; Cieplak, P.; Cornell, W.; Kollman, P. A., A well-behaved electrostatic potential based method using charge restraints for deriving atomic charges: the RESP model. *J. Phys. Chem.* **1993**, 97, 10269-10280.

133. Dupradeau, F.-Y.; Pigache, A.; Zaffran, T.; Savineau, C.; Lelong, R.; Grivel, N.; Lelong, D.; Rosanski, W.; Cieplak, P., The REd. Tools: Advances in RESP and ESP charge derivation and force field library building. *Phys. Chem. Chem. Phys.* **2010**, 12, 7821-7839.

134. Vanquelef, E.; Simon, S.; Marquant, G.; Garcia, E.; Klimerak, G.; Delepine, J. C.; Cieplak, P.; Dupradeau, F.-Y., RED Server: a web service for deriving RESP and ESP charges and building force field libraries for new molecules and molecular fragments. *Nucleic Acids Res.* **2011**, 39, W511-W517.

135. Wang, F.; Becker, J.-P.; Cieplak, P.; Dupradeau, F.-Y. RED Python: Object oriented programming for Amber force fields. In Abstracts of Papers of the American Chemical Society, 2014; AMER CHEMICAL SOC 1155 16TH ST, NW, WASHINGTON, DC 20036 USA: 2014; Vol. 247.

136. Wang, J.; Wolf, R. M.; Caldwell, J. W.; Kollman, P. A.; Case, D. A., Development and testing of a general amber force field. *J. Comput. Chem.* **2004**, 25, 1157-1174.

137. Wang, J.; Wang, W.; Kollman, P. A.; Case, D. A., Automatic atom type and bond type perception in molecular mechanical calculations. *J. Mol. Graph. Model.* **2006**, 25, 247-260.

138. Olsson, M. H.; Søndergaard, C. R.; Rostkowski, M.; Jensen, J. H., PROPKA3: consistent treatment of internal and surface residues in empirical p K a predictions. *J. Chem. Theory Comput.* **2011**, 7, 525-537.

139. Søndergaard, C. R.; Olsson, M. H.; Rostkowski, M.; Jensen, J. H., Improved treatment of ligands and coupling effects in empirical calculation and rationalization of p K a values. *J. Chem. Theory Comput.* **2011**, 7, 2284-2295.

140. Schafmeister, C.; Ross, W.; Romanovski, V., LEaP. *University of California, San Francisco* **1995**.

141. Case, D. A.; Aktulga, H. M.; Belfon, K.; Ben-Shalom, I.; Brozell, S. R.; Cerutti, D. S.; Cheatham III, T. E.; Cruzeiro, V. W. D.; Darden, T. A.; Duke, R. E., *Amber 2021*. University of California, San Francisco: 2021.

142. Jorgensen, W. L.; Chandrasekhar, J.; Madura, J. D.; Impey, R. W.; Klein, M. L., Comparison of simple potential functions for simulating liquid water. *J. Chem. Phys.* **1983**, 79, 926-935.

143. Maier, J. A.; Martinez, C.; Kasavajhala, K.; Wickstrom, L.; Hauser, K. E.; Simmerling, C., ff14SB: improving the accuracy of protein side chain and backbone parameters from ff99SB. *J. Chem. Theory Comput.* **2015**, 11, 3696-3713.

144. Salomon-Ferrer, R.; Gotz, A. W.; Poole, D.; Le Grand, S.; Walker, R. C., Routine microsecond molecular dynamics simulations with AMBER on GPUs. 2. Explicit solvent particle mesh Ewald. *J. Chem. Theory Comput.* **2013**, 9, 3878-3888.

145. Ryckaert, J.-P.; Ciccotti, G.; Berendsen, H. J., Numerical integration of the cartesian equations of motion of a system with constraints: molecular dynamics of n-alkanes. *J. Comput. Phys.* **1977**, 23, 327-341.

146. Berendsen, H. J.; Postma, J. v.; Van Gunsteren, W. F.; DiNola, A.; Haak, J. R., Molecular dynamics with coupling to an external bath. *J. Chem. Phys.* **1984**, 81, 3684-3690.

147. Zwanzig, R., Nonlinear generalized Langevin equations. *J. Stat. Phys.* **1973**, 9, 215-220.

148. Loncharich, R. J.; Brooks, B. R.; Pastor, R. W., Langevin dynamics of peptides: The frictional dependence of isomerization rates of N-acetylalanyl-N′-methylamide. *Biopolymers: Original Research on Biomolecules* **1992**, 32, 523-535.

149. Gillespie, D. T., The chemical Langevin equation. *J. Chem. Phys.* **2000**, 113, 297-306.

150. Davidchack, R. L.; Handel, R.; Tretyakov, M., Langevin thermostat for rigid body dynamics. *J. Chem. Phys.* **2009**, 130, 234101.

151. Essmann, U.; Perera, L.; Berkowitz, M. L.; Darden, T.; Lee, H.; Pedersen, L. G., A smooth particle mesh Ewald method. *J. Chem. Phys.* **1995**, 103, 8577-8593.

152. Roe, D. R.; Cheatham III, T. E., PTRAJ and CPPTRAJ: software for processing and analysis of molecular dynamics trajectory data. *J. Chem. Theory Comput.* **2013**, 9, 3084-3095.

153. Bakan, A.; Meireles, L. M.; Bahar, I., ProDy: protein dynamics inferred from theory and experiments. *Bioinformatics* **2011**, 27, 1575-1577.

154. Likas, A.; Vlassis, N.; Verbeek, J. J., The global k-means clustering algorithm. *Pattern Recognit* **2003**, 36, 451-461.

155. Kollman, P. A.; Massova, I.; Reyes, C.; Kuhn, B.; Huo, S.; Chong, L.; Lee, M.; Lee, T.; Duan, Y.; Wang, W., Calculating structures and free energies of complex molecules: combining molecular mechanics and continuum models. *Acc. Chem. Res.* **2000**, 33, 889-897.

156. Wang, W.; Donini, O.; Reyes, C. M.; Kollman, P. A., Biomolecular simulations: recent developments in force fields, simulations of enzyme catalysis, protein-ligand, protein-protein, and protein-nucleic acid noncovalent interactions. *Annu. Rev. Biophys. Biomol. Struct.* **2001**, 30, 211-243.

157. Wang, J.; Hou, T.; Xu, X., Recent advances in free energy calculations with a combination of molecular mechanics and continuum models. *Curr. Comput. Aided Drug Des.* **2006**, 2, 287-306.

158. Hou, T.; Wang, J.; Li, Y.; Wang, W., Assessing the performance of the MM/PBSA and MM/GBSA methods. 1. The accuracy of binding free energy calculations based on molecular dynamics simulations. *J. Chem. Inf. Model.* **2011**, 51, 69-82.

159. Hou, T.; Wang, J.; Li, Y.; Wang, W., Assessing the performance of the molecular mechanics/Poisson Boltzmann surface area and molecular mechanics/generalized Born surface area methods. II. The accuracy of ranking poses generated from docking. *J. Comput. Chem.* **2011**, 32, 866-877.

160. Muzzioli, E.; Del Rio, A.; Rastelli, G., Assessing Protein Kinase Selectivity with Molecular Dynamics and MM-PBSA Binding Free Energy Calculations. *Chem. Biol. Drug Des.* **2011**, 78, 252-259.

161. Xu, L.; Li, Y.; Li, L.; Zhou, S.; Hou, T., Understanding microscopic binding of macrophage migration inhibitory factor with phenolic hydrazones by molecular docking, molecular dynamics simulations and free energy calculations. *Mol. Biosyst.* **2012**, 8, 2260-2273.

162. Sun, H.; Duan, L.; Chen, F.; Liu, H.; Wang, Z.; Pan, P.; Zhu, F.; Zhang, J. Z.; Hou, T., Assessing the performance of MM/PBSA and MM/GBSA methods. 7. Entropy effects on the performance of end-point binding free energy calculation approaches. *Phys. Chem. Chem. Phys.* **2018**, 20, 14450-14460.

163. Chen, J.; Zhang, S.; Wang, W.; Sun, H.; Zhang, Q.; Liu, X., Binding of inhibitors to BACE1 affected by pH-dependent protonation: An exploration from multiple replica Gaussian accelerated molecular dynamics and MM-GBSA calculations. *ACS Chem. Neurosci.* **2021**, 12, 2591-2607.

164. Ongaro, A.; Oselladore, E.; Memo, M.; Ribaudo, G.; Gianoncelli, A., Insight into the LFA-1/SARS-CoV-2 Orf7a complex by protein–protein docking, molecular dynamics, and MM-GBSA calculations. *J. Chem. Inf. Model.* **2021**, 61, 2780-2787.

165. Tuccinardi, T., What is the current value of MM/PBSA and MM/GBSA methods in drug discovery? *Expert Opin. Drug Discovery* **2021**, 16, 1233-1237.

166. Naseem-Khan, S.; Berger, M. B.; Leddin, E. M.; Maghsoud, Y.; Cisneros, G. A., Impact of Remdesivir Incorporation along the Primer Strand on SARS-CoV-2 RNA-Dependent RNA Polymerase. *J. Chem. Inf. Model.* **2022**, 62, 2456-2465.

167. Kratz, E. G.; Walker, A. R.; Lagardère, L.; Lipparini, F.; Piquemal, J. P.; Andrés Cisneros, G., LICHEM: A QM/MM program for simulations with multipolar and polarizable force fields. *J. Comput. Chem.* **2016**, 37, 1019-1029.

168. Gökcan, H.; Vázquez-Montelongo, E. A.; Cisneros, G. A., LICHEM 1.1: recent improvements and new capabilities. *J. Chem. Theory Comput.* **2019**, 15, 3056-3065.

169. Frisch, M. J.; Trucks, G. W.; Schlegel, H. B.; Scuseria, G. E.; Robb, M. A.; Cheeseman, J. R.; Scalmani, G.; Barone, V.; Petersson, G. A.; Nakatsuji, H.; Li, X.; Caricato, M.; Marenich, A. V.; Bloino, J.; Janesko, B. G.; Gomperts, R.; Mennucci, B.; Hratchian, H. P.; Ortiz, J. V.; Izmaylov, A. F.; Sonnenberg, J. L.; Williams; Ding, F.; Lipparini, F.; Egidi, F.; Goings, J.; Peng, B.; Petrone, A.; Henderson, T.; Ranasinghe, D.; Zakrzewski, V. G.; Gao, J.; Rega, N.; Zheng, G.; Liang, W.; Hada, M.; Ehara, M.; Toyota, K.; Fukuda, R.; Hasegawa, J.; Ishida, M.; Nakajima, T.; Honda, Y.; Kitao, O.; Nakai, H.; Vreven, T.; Throssell, K.; Montgomery Jr., J. A.; Peralta, J. E.; Ogliaro, F.; Bearpark, M. J.; Heyd, J. J.; Brothers, E. N.; Kudin, K. N.; Staroverov, V. N.; Keith, T. A.; Kobayashi, R.; Normand, J.; Raghavachari, K.; Rendell, A. P.; Burant, J. C.; Iyengar, S. S.; Tomasi, J.; Cossi, M.; Millam, J. M.; Klene, M.; Adamo, C.; Cammi, R.; Ochterski, J. W.; Martin, R. L.; Morokuma, K.; Farkas, O.; Foresman, J. B.; Fox, D. J. *Gaussian 16 Rev. C.01*, Wallingford, CT, 2016.

170. Rackers, J. A.; Wang, Z.; Lu, C.; Laury, M. L.; Lagardère, L.; Schnieders, M. J.; Piquemal, J.-P.; Ren, P.; Ponder, J. W., Tinker 8: software tools for molecular design. *J. Chem. Theory Comput.* **2018**, 14, 5273-5289.

171. Weigend, F.; Ahlrichs, R., Balanced basis sets of split valence, triple zeta valence and quadruple zeta valence quality for H to Rn: Design and assessment of accuracy. *Phys. Chem. Chem. Phys.* **2005**, 7, 3297-3305.

172. Andrae, D.; Haeussermann, U.; Dolg, M.; Stoll, H.; Preuss, H., Energy-adjustedab initio pseudopotentials for the second and third row transition elements. *Theor. Chim. Acta* **1990**, 77, 123-141.

173. Maghsoud, Y.; Vázquez-Montelongo, E. A.; Yang, X.; Liu, C.; Jing, Z.; Lee, J.; Harger, M.; Smith, A. K.; Espinoza, M.; Guo, H.-F., Computational Investigation of a Series of Small Molecules as Potential Compounds for Lysyl Hydroxylase-2 (LH2) Inhibition. *J. Chem. Inf. Model.* **2023**, 63, 986-1001.

174. Simon, S.; Duran, M.; Dannenberg, J., How does basis set superposition error change the potential surfaces for hydrogen-bonded dimers? *J. Chem. Phys.* **1996**, 105, 11024-11031.

175. Galano, A.; Alvarez–Idaboy, J. R., A new approach to counterpoise correction to BSSE. *J. Comput. Chem.* **2006**, 27, 1203-1210.

176. Dzib, E.; Cabellos, J. L.; Ortíz-Chi, F.; Pan, S.; Galano, A.; Merino, G., Eyringpy: A program for computing rate constants in the gas phase and in solution. *Int. J. Quantum Chem.* **2019**, 119, e25686.

177. E. Dzib, A. Q., F. Ortiz-Chi, G. Merino, Eyringpy 2.0. *Cinvestav, Merida, Yucatan* **2021**.

178. Collins, F. C.; Kimball, G. E., Diffusion-controlled reaction rates. *J. Colloid Sci.* **1949**, 4, 425-437.

179. Johnson, E. R.; Keinan, S.; Mori-Sánchez, P.; Contreras-García, J.; Cohen, A. J.; Yang, W., Revealing noncovalent interactions. *J. Am. Chem. Soc.* **2010**, 132, 6498-6506.

180. Lu, T.; Chen, F., Multiwfn: a multifunctional wavefunction analyzer. *J. Comput. Chem.* **2012**, 33, 580-592.

181. Becke, A. D.; Edgecombe, K. E., A simple measure of electron localization in atomic and molecular systems. *J. Chem. Phys.* **1990**, 92, 5397-5403.

182. YANG, S.; XU, G.-Y.; HAN, J.-P.; BING, H.; DOU, H.; ZHANG, X.-G., Nitrogen-doped porous carbon derived from dopamine-modified polypyrrole and its electrochemical capacitive behavior. *Acta Phys.-Chim. Sin.* **2015**, 31, 685-692.

183. LU, T.; CHEN, F.-W., Meaning and functional form of the electron localization function. *Acta Phys.-Chim. Sin.* **2011**, 27, 2786-2792.

184. Humphrey, W.; Dalke, A.; Schulten, K., VMD: visual molecular dynamics. *J. Mol. Graph.* **1996**, 14, 33-38.

185. Maghsoud, Y.; Jayasinghe-Arachchige, V. M.; Kumari, P.; Cisneros, G. A.; Liu, J., Leveraging QM/MM and Molecular Dynamics Simulations to Decipher the Reaction Mechanism of the Cas9 HNH Domain to Investigate off-Target Effects. **2023**.

186. Graham, S. E.; Syeda, F.; Cisneros, G. A. s., Computational prediction of residues involved in fidelity checking for DNA synthesis in DNA polymerase I. *Biochemistry* **2012**, 51, 2569-2578.

187. Dewage, S. W.; Cisneros, G. A., Computational analysis of ammonia transfer along two intramolecular tunnels in Staphylococcus aureus glutamine-dependent amidotransferase (GatCAB). *J. Phys. Chem. B* **2015**, 119, 3669-3677.

188. Walker, A. R.; Cisneros, G. A. s., Computational simulations of DNA polymerases: detailed insights on structure/function/mechanism from native proteins to cancer variants. *Chem. Res. Toxicol.* **2017**, 30, 1922-1935.

189. Nagamatsu, T.; Fujita, T.; Endo, K., Novel xanthine oxidase inhibitor studies. Part 3. 1 Convenient and general syntheses of 3-substituted 7 H-pyrazolo [4, 3-e]-1, 2, 4-triazolo [4, 3-c] pyrimidin-5 (6 H)-ones as a new class of potential xanthine oxidase inhibitors. *J. Chem. Soc., Perkin Trans. 1* **2000**, 33-42.

190. Boudet, N.; Knochel, P., Chemo-and regioselective functionalization of uracil derivatives. Applications to the synthesis of oxypurinol and emivirine. *Organic letters* **2006**, 8, 3737-3740.

191. Day, R. O.; Graham, G. G.; Hicks, M.; McLachlan, A. J.; Stocker, S. L.; Williams, K. M., Clinical pharmacokinetics and pharmacodynamics of allopurinol and oxypurinol. *Clin. Pharmacokinet.* **2007**, 46, 623-644.

192. Singla, P.; Luxami, V.; Singh, R.; Tandon, V.; Paul, K., Novel pyrazolo [3, 4-d] pyrimidine with 4-(1H-benzimidazol-2-yl)-phenylamine as broad spectrum anticancer agents: Synthesis, cell based assay, topoisomerase inhibition, DNA intercalation and bovine serum albumin studies. *Eur. J. Med. Chem.* **2017**, 126, 24-35.

193. El-Mekabaty, A.; Etman, H. A.; Mosbah, A.; Fadda, A. A., Synthesis, In Vitro Cytotoxicity and Bleomycin-Dependent DNA Damage Evaluation of Some Heterocyclic-Fused Pyrimidinone Derivatives. *ChemistrySelect* **2020**, 5, 4856-4861.

194. Plouvier, B. M. C.; Choi, L. S. L. Crystal salt of xanthine oxidase inhibitors. WO2006083687A1, 2006.

195. Chalmers, R.; Parker, R.; Simmonds, H.; Snedden, W.; Watts, R., The conversion of 4-hydroxypyrazolo-[3, 4-d] pyrimidine (allopurinol) into 4, 6-dihydroxypyrazolo [3, 4-d] pyrimidine (oxipurinol) in vivo in the absence of xanthine–oxygen oxidoreductase. *Biochem. J.* **1969**, 112, 527-532.

196. Nelson, D. J.; Buggé, C. J.; Krasny, H. C.; Elion, G. B., Formation of nucleotides of [6-14C] allopurinol and [6-14C] oxipurinol in rat tissues and effects on uridine nucleotide pools. *Biochem. Pharmacol.* **1973**, 22, 2003-2022.

197. Stevenson, A.; Silcock, S.; Scott, J., Absence of chromosome damage in human lymphocytes exposed to allopurinol and oxipurinol. *Ann. Rheum. Dis.* **1976**, 35, 143-147.

198. Spector, T., Inhibition of urate production by allopurinol. *Biochem. Pharmacol.* **1977**, 26, 355-358.

199. Williams, J. W.; Bray, R., Kinetic and epr studies on the inhibition of xanthine oxidase by alloxanthine (1 H-pyrazolo [3, 4-d] pyrimidine-4, 6-diol). *Biochem. J.* **1981**, 195, 753-760.

200. Shaw, M.; Parsons, D., Absorption and metabolism of allopurinol and oxypurinol by rat jejunum in vitro: effects on uric acid transport. *Clin. Sci.* **1984**, 66, 257-267.

201. Hernández, R.; Orozco, M.; Luque, F. J., Tautomerism of xanthine and alloxanthine: A model for substrate recognition by xanthine oxidase. *J. Comput. Aided Mol. Des.* **1996**, 10, 535-544.

202. Bergmann, F.; Frank, A.; Neiman, Z., Studies on the chemical reactivity and the physical properties of allopurinol (pyrazolo [3, 4-d] pyrimidin-4-one) and related compounds. *J. Chem. Soc., Perkin Trans. 1* **1979**, 2795-2802.

203. Hänggi, G.; Schmalle, H.; Dubler, E., N (8)-coordinating allopurinol: structure of bis (allopurinol) triaqua (sulfato) copper (II) hydrate. *Acta Crystallographica Section C: Crystal Structure Communications* **1991**, 47, 1609-1614.

204. Prusiner, P.; Sundaralingam, M., Stereochemistry of nucleic acids and their constituents. XXIX. Crystal and molecular structure of allopurinol, a potent inhibitor of xanthine oxidase. *Acta Crystallographica Section B: Structural Crystallography and Crystal Chemistry* **1972**, 28, 2148-2152.

205. Nishino, T.; Okamoto, K., Mechanistic insights into xanthine oxidoreductase from development studies of candidate drugs to treat hyperuricemia and gout. *JBIC, J. Biol. Inorg. Chem.* **2015**, 20, 195-207.

206. Spector, T.; Johns, D., Stoichiometric inhibition of reduced xanthine oxidase by hydroxypyrazolo [3, 4-d] pyrimidines. *J. Biol. Chem.* **1970**, 245, 5079-5085.

207. Krenitsky, T. A.; Spector, T.; Hall, W. W., Xanthine oxidase from human liver: purification and characterization. *Arch. Biochem. Biophys.* **1986**, 247, 108-119.

208. Pauff, J. M.; Cao, H.; Hille, R., Substrate orientation and catalysis at the Molybdenum site in xanthine oxidase. *J. Biol. Chem.* **2009**, 284, 8760-8767.

209. Ilich, P.; Hille, R., Tautomerization of the substrate heterocycle in the course of the reaction of xanthine oxidase. *Inorg. Chim. Acta* **1997**, 263, 87-93.

210. Pauff, J. M.; Hemann, C. F.; Jünemann, N.; Leimkühler, S.; Hille, R., The role of arginine 310 in catalysis and substrate specificity in xanthine dehydrogenase from Rhodobacter capsulatus. *J. Biol. Chem.* **2007**, 282, 12785-12790.

211. Leimkühler, S.; Stockert, A. L.; Igarashi, K.; Nishino, T.; Hille, R., The role of active site glutamate residues in catalysis of Rhodobacter capsulatus xanthine dehydrogenase. *J. Biol. Chem.* **2004**, 279, 40437-40444.

212. Glatigny, A.; Hof, P.; Romão, M. J.; Huber, R.; Scazzocchio, C., Altered specificity mutations define residues essential for substrate positioning in xanthine dehydrogenase. *J. Mol. Biol.* **1998**, 278, 431-438.

213. Stiburkova, B.; Krijt, J.; Vyletal, P.; Bartl, J.; Gerhatova, E.; Korinek, M.; Sebesta, I., Novel mutations in xanthine dehydrogenase/oxidase cause severe hypouricemia: biochemical and molecular genetic analysis in two Czech families with xanthinuria type I. *Clin. Chim. Acta* **2012**, 413, 93-99.

214. Xu, T.; Xie, X.; Zhang, Z.; Zhao, N.; Deng, Y.; Li, P., A novel mutation in xanthine dehydrogenase in a case with xanthinuria in Hunan province of China. *Clin. Chim. Acta* **2020**, 504, 168-171.

215. Kudo, M.; Moteki, T.; Sasaki, T.; Konno, Y.; Ujiie, S.; Onose, A.; Mizugaki, M.; Ishikawa, M.; Hiratsuka, M., Functional characterization of human xanthine oxidase allelic variants. *Pharmacogenet. Genomics* **2008**, 18, 243-251.

216. Ichida, K.; Amaya, Y.; Kamatani, N.; Nishino, T.; Hosoya, T.; Sakai, O., Identification of two mutations in human xanthine dehydrogenase gene responsible for classical type I xanthinuria. *J. Clin. Invest.* **1997**, 99, 2391-2397.

217. Arikyants, N.; Sarkissian, A.; Hesse, A.; Eggermann, T.; Leumann, E.; Steinmann, B., Xanthinuria type I: a rare cause of urolithiasis. *Pediatr. Nephrol.* **2007**, 22, 310-314.

218. Gok, F.; Ichida, K.; Topaloglu, R., Mutational analysis of the xanthine dehydrogenase gene in a Turkish family with autosomal recessive classical xanthinuria. *Nephrol., Dial., Transplant.* **2003**, 18, 2278-2283.

219. Tanaka, K.-i.; Kanazawa, I.; Yamasaki, H.; Hasegawa, H.; Ichida, K.; Sugimoto, T., Xanthinuria type I with a novel mutation of xanthine dehydrogenase. *Am. J. Med. Sci.* **2015**, 350, 155-156.

220. Johns, D. G., Anomalous differential effects of 4-hydroxypyrazolo (3, 4-d)-pyrimidine on electron transfer from xanthine oxidase to molecular oxygen and to acceptor dyes. *Biochem. Biophys. Res. Commun.* **1968**, 31, 197-202.

221. Spector, T.; Johns, D., Oxidation of 4-hydroxypyrazolo (3, 4-d) pyrimidine by xanthine oxidase: The route of electron transfer from substrate to acceptor dyes. *Biochem. Biophys. Res. Commun.* **1968**, 32, 1039-1044.